Utilisation of staphylococcal immune evasion protein Sbi as a novel vaccine adjuvant

Yang, Y. §[1], Back, CR.§[1], Gräwert, MA.[2], Wahid, AA.[1], Denton, H.[3], Kildani, R.[3], Paulin, J.[3], Wörner, K.[4], Kaiser, W.[4], Svergun, DI.[2], Sartbaeva, A.[5] Watts, AG.[6], Marchbank, KJ.[3]*, and van den Elsen, JMH[1]*.

[1]Department of Biology and Biochemistry, University of Bath, Bath, UK
[2]European Molecular Biology Laboratory, Hamburg Unit
c/o Deutsches Elektronen-Synchrotron, Hamburg, Germany
[3]Institute of Cellular Medicine, Newcastle University, Newcastle-upon-Tyne, UK
[4]Dynamic Biosensors GmbH, Martinsried, Germany
[5]Department of Chemistry, University of Bath, Bath, UK
[6]Department of Pharmacy and Pharmacology, University of Bath, Bath, UK

§Contributed equally to this work

*Co-Corresponding author addresses: Jean van den Elsen (j.m.h.v.elsen@bath.ac.uk) and Kevin James Marchbank (Kevin.marchbank@ncl.ac.uk)

Abstract

Co-ligation of the B cell antigen receptor with complement receptor 2 on B-cells via a C3d-opsonised antigen complex significantly lowers the threshold required for B cell activation. Consequently, fusions of antigens with C3d polymers have shown great potential in vaccine design. However, these linear arrays of C3d multimers do not mimic the natural opsonisation of antigens with C3d. Here we investigate the potential of using the unique complement activating characteristics of Staphylococcal immune-evasion protein Sbi to develop a pro-vaccine approach that spontaneously coats antigens with C3 degradation products in a natural way. We show that Sbi rapidly triggers the alternative complement pathway through recruitment of complement regulators, forming a tripartite complex that acts as a competitive antagonist of factor H, resulting in enhanced complement consumption. These functional results are corroborated by the structure of this complement activating Sbi-III-IV:C3d:FHR-1 complex. Finally, we demonstrate that Sbi, fused with *Mycobacterium tuberculosis* antigen Ag85b, causes efficient opsonisation with C3 fragments, thereby enhancing the immune response significantly beyond that of Ag85b alone, providing proof of concept for our pro-vaccine approach.

Introduction

Opsonisation of an antigen with C3d(g), the final degradation product of complement component C3, results in the co-ligation of the B cell antigen receptor and complement receptor 2 (CR2) on B cells, thereby instigating a profound molecular adjuvant effect, i.e. this co-ligation of receptor complexes lowers the threshold of antigen required for B cell activation by up to 10,000 fold [1-3]. Furthermore, as CR2 is also expressed highly on follicular dendritic cells (FDCs) [4] the presence of C3d(g) on the antigen allows it to be trafficked onto and trapped at the surface of these cells [5]. This provides an essential depot of antigen to support the germinal center reaction and maintain the ongoing immune response including the generation of high affinity antibodies and memory B-cells [3, 4, 6]. B cells can also have an important role as antigen presenting cells (APCs) [7, 8] and have been shown to contribute to T-helper cell priming [9, 10] and therefore, antigen-C3d-CR2 interactions play a key role in humoral immunity [5]. Additionally, C3d activation of T helper cells has also been described in a CR2 independent manner [11], underlining the importance of C3d opsonisation in stimulation of the immune system to respond.

Not surprisingly, this functionality led to the idea that recombinant versions of C3d would make an ideal natural adjuvant and to the subsequent design of linear polymers of human C3d [12]. Indeed, these linear arrays of C3d multimers (3-mer to 20-mer) when fused directly to an antigen can act as potent activators of human B-cells. However, they do not mimic the natural opsonisation of

antigens by C3d at a molecular level and do not always enhance immune responses [13]. After activation of C3, C3b attaches directly to the antigen surface via the reactive thioester on the convex face of the protein's thioester domain (TED). In the presence of complement regulators (factor I (FI) and its co-factors, such as factor H (FH) and CR1) this is rapidly converted to iC3b and then to C3d, exposing the concave CR2 binding site of the TED fragment away from the antigen surface [14]. It is likely that multiple iC3b/C3d molecules attach to complex antigens/pathogen surfaces during the initial activation phases of complement, creating high-avidity binding site for complement fragment receptors.

In the last two decades, structural biology has helped to unveil many of the molecular aspects that are crucial for the activation and regulation of the complement system. Most notable are the crystal structures of the central complement component activation states, native C3 [15], activated C3b and inactive C3c [16]. The structure of C3b in complex with factors B and D [17] subsequently revealed a detailed view of the alternative pathway C3 convertase assembly and its activation, leading to the amplified cleavage of C3 molecules that result in opsonisation and clearance of microbial pathogens and host debris. The covalent attachment of C3b to surfaces does not discriminate between self or non-self surfaces and requires tight regulation to protect host surfaces. Structures of C3b in complex with FH domains 1-4 [18] and domains 19-20 [19, 20] provided insights into protection of host cells [21] and demonstrated how

104 factor H-related proteins (FHRs) function as competitive antagonists of FH,
105 modulating complement activation and providing improved discrimination of
106 self and non-self surfaces [22]. The subsequent structure of the complex of C3b,
107 FH_{1-4} and regulator factor I [23] improved our understanding in the proteolytic
108 cleavage of C3b to the late-stage opsonins iC3b or C3dg and provided the basis
109 for the regulator-dependent differences in processing and immune recognition
110 of opsonized material.

111 Here we investigate the potential to harness the unique
112 complement-stimulatory characteristics of *Staphylococcus aureus*
113 immunomodulator Sbi to develop 'pro-vaccines'. Sbi components would trigger
114 natural complement activation in the host and coat antigen surfaces with
115 complement component C3 degradation products, thereby enhancing the degree
116 of immunogenicity of target antigens. Research from our lab previously revealed
117 that Sbi contains two domains (III and IV), which bind to the central complement
118 component C3 and cause futile fluid phase consumption of this component [24].
119 Therefore, these two domains of Sbi offer the potential to not only coat an
120 antigen with the natural adjuvant C3d, but also to generate anaphylatoxins and
121 the full range of C3 opsonins. Such an approach has the clear potential to activate
122 many immune cells unlike recombinant C3d fragment-based adjuvants of the
123 past, that, due to the restricted expression pattern of CR2, were largely focused
124 to B cells. Furthermore, the direct activation of complement close to the target
125 antigen (with the associated anaphylatoxin generation) may be critical for

126 generating appropriate inflammatory immune responses, both humoral and
127 cellular; needed to immunise against complex pathogenic targets.

128 In this study we first investigate the molecular mode of action of Sbi-III-IV
129 and evaluate the importance of the tripartite complex formation between Sbi,
130 C3d and complement regulators factor H (FH) or factor H-related proteins (FHRs)
131 for complement activation. Based on these findings, we then tested whether our
132 pro-vaccine strategy would be successful by using *Mycobacterium tuberculosis*
133 antigen 85b (Ag85b) as a model antigen in a fusion construct containing Sbi
134 domains III and IV. We show that this Sbi-Ag85b conjugate is opsonized by C3
135 degradation products in serum, and when administered to mice, leads to an
136 enhanced immune response *in vivo,* but only in mice that possess C3 and
137 complement receptor 1 and 2, demonstrating proof of concept for this adjuvant
138 compound.

Results:

Sbi-III-IV triggers C3 consumption via activation of the alternative complement pathway, forming a covalent adduct with C3b

To investigate the molecular details of the C3 futile consumption caused by Sbi, a protein construct consisting of domains III and IV (Sbi-III-IV) was incubated with normal human serum (NHS) and analyzed using western blotting. As seen previously [24], we found that Sbi-III-IV-induced C3 consumption results in the deposition of metastable C3b molecules onto serum proteins, causing the formation of high molecular weight C3b covalent adduct species with serum proteins (Figure 1a). Immuno-blotting analyses using a polyclonal anti-Sbi antibody (Figure 1b) reveals that a small fraction of Sbi-III-IV molecule also forms a covalent adduct with a nascent C3b molecule that is subsequently converted into a smaller Sbi-iC3b adduct as a result of proteolytic processing by serum proteases. In addition, we show that Sbi-III-IV-induced C3 consumption coincides with the release of the C3a anaphylatoxin fragment (Figure 1c), and the proteolytic activation of factor B (FB) (Figure 1d), confirming the alternative complement pathway as the driving force behind this process. Pre-incubation of serum with Sbi-III-IV results in the loss of serum hemolytic ability caused by the futile consumption of fluid C3 (Figure 1e). Without pre-incubation, the Sbi-III-IV construct does not protect rabbit erythrocytes from lysis in NHS under AP conditions.

Sbi domain III residue K173 is essential for complement consumption

In order to gain understanding of the individual roles of Sbi domains III and IV in AP activation, a systematic site-directed mutagenesis approach was used, mainly focusing on charged and polar amino acids (for details see Supplementary Table S1 and Figure S1). Functional screening of these mutants identified K173, located within Sbi domain III (Figure 1f), as an essential contributor to triggering C3 consumption. Sbi mutant K173A shows no complement activation after 30 minutes incubation with human serum, demonstrating a comparable complement activation defect to the previously identified C3d binding mutant R231A [24, 25] (Figure 1f and g), located in Sbi domain IV. Assessment of the C3d binding affinity, using *switch*SENSE (Table 1 and Supplementary Figure S2A), shows that contrary to R231A the C3d binding capacity of K173A is unaffected, indicating it is essential for the role for domain III in the futile consumption of C3. Interestingly, our *switch*SENSE analyses of the C3d binding characteristics also shows a reduced hydrodynamic diameter for K173A compared to WT and the C3d impaired binding mutant R231A, indication that this mutation in domain III results in a more compact Sbi:C3d complex (Table 2 and Supplementary Figure S2B). A more detailed structural analysis of these conformational changes follows below.

Sbi-III-IV enhances binding of FH or FHRs to C3 breakdown products

In a previous study, we reported that Sbi-III-IV binds C3 isoforms in

combination with the C-terminal part of FH (FH_{19-20}), forming tripartite complexes [26]. Many FHRs share SCR modules with high FH_{19-20} sequence identity [22] particularly FHR1 which has been demonstrated to have significant complement dysregulation potential [21]. Thus, we investigated the potential role for Sbi-III-IV in mediating the formation of tripartite complexes with C3 fragments and FHR-1, FHR-2 or FHR-5.

On a C3b opsonised surface plasmon resonance (SPR) sensor chip, the presence of wild-type Sbi-III-IV clearly enhanced the binding of FH, FHR-1, FHR-2, FHR-5 as well as FH_{19-20} (at fixed concentrations of 100, 12.5, 20, 25 and 20nM, respectively) to the surface in a concentration dependent manner (Figure 2a). However, in the case of the K173A mutant, tripartite complex formation with FH or FHR-1, 2, 5 or FH_{19-20} is significantly impaired, showing decreased binding and more rapid dissociation compared to WT Sbi-III-IV (Figure 2b and 2c). We also co-injected Sbi-III-IV with FH or FHR-1, flowing opsonized iC3b or amine-coupled C3d(g) across the surface. On these surfaces, the fold-changes in FH (or FHR-1) binding levels were also enhanced even at reduced Sbi-III-IV concentration (Supplementary Figures S3A-D).

Sbi-III-IV acts as a competitive antagonist of FH via the recruitment of FHRs

Our SPR data, described above, show that Sbi-III-IV enables FH or FHR-1, 2 and 5 binding to the C3 activation fragment C3b and late-stage proteolytic fragments iC3b and C3d(g). To further our understanding of the mechanism of

205 FH or FHR recruitment and the contribution of these tripartite complexes to AP
206 complement activation, we used a rabbit erythrocyte haemolytic assay. In the
207 presence of Sbi-III-IV and endogenous FH (and FHRs), in NHS, addition of
208 recombinant FHR-1 or FHR-2 resulted in significantly enhanced C3 consumption
209 (Figure 3a), as evidenced by the reduction in erythrocyte lysis in a concentration
210 dependent manner. In the absence of Sbi-III-IV only baseline C3 consumption
211 was observed. Although FHR-5 alone can reduce erythrocyte lysis in a
212 concentration dependent manner, as described previously [27], in the presence
213 of Sbi-III-IV C3 consumption by FHR-5 is clearly enhanced (Figure 3b). As
214 predicted, the results in Figure 3c indicate that the observed reduction in
215 erythrocyte lysis caused by C3 fluid phase consumption, in the case of FHR1 and
216 likely the remaining FHRs, is mediated by the C-terminal SCR domains of the
217 protein rather than the N-terminal domains.

218 Whilst our SPR and rabbit erythrocyte assay clearly indicate that *in vitro*
219 Sbi-III-IV can recruit FHRs in tripartite complexes with C3b and thereby enhance
220 fluid phase complement consumption, it has to be taken into account that the
221 physiological molar concentrations of FHR-1, 2 and 5 are 13-164 fold less than
222 that of FH [21, 28]. To further investigate the potential competitive binding
223 between FH and the FHRs in Sbi-III-IV mediated tripartite complexes, we used an
224 ELISA-based assay where we applied FH (25 nM) and Sbi-III-IV (1 μM, in the
225 presence of a concentration range of FHRs (9.3 – 150nM)) onto a C3b coated
226 plate. Subsequently, we assessed the percentage of FH bound using monoclonal

antibody OX-24. Figure 3d shows that FHR-1 can compete with FH to bind C3b, decreasing the percentage of residual FH bound to C3b from ~70% at the lowest FHR-1 concentration to ~30% at the highest concentration. In the presence of Sbi-III-IV WT this effect is dramatically increased with only ~25% residual FH bound at the lowest FHR-1 concentration, reducing to ~0% at the highest FHR-1 concentration (Figure 3e). These results clearly indicate that Sbi-III-IV can preferentially recruit FHR-1 to form a tripartite complex with C3b. Similarly, enhancement of recruitment was observed with FHR-5 and fragment FH_{19-20} but only weakly with FHR-2. Although unable to activate complement, Sbi-III-IV mutant K173A is still able to compete for the binding of FHR-1 in the presence of FH, but its ability to enhance binding of FHR-2 and FHR-5 to C3b is clearly affected (Figure 3f).

To assess the potential AP de-regulatory roles of the Sbi-III-IV mediated tripartite complexes. We subjected them to a novel C3 convertase decay acceleration activity (DAA) assay and a fluid phase C3b co-factor activity (CFA) assay [29, 30]. We demonstrated that in absence of Sbi, FHR-1 failed to antagonise FH efficiently and show a difference in the level of C3 convertase formation (Figure 3g). Co-injection of FHR-1 and -5 shows reduced C3 convertase formation, which is in accordance with the results from a previous study [31]. However, the presence of Sbi (2μM) potentiates the FH antagonising effect of FHR-1, and to a lesser extent that of FHR-5, at a physiologically relevant concentration ratio (FH 2000 nM: FHR-1 200 nM : FHR-5 20 nM), resulting in

249 increased C3 convertase formation on a C3b surface (Figure 3h). The baseline
250 C3b breakdown rate was acquired in the presence of FH (0.160μM) and FI
251 (0.017μM), and subsequent measurements were performed in the presence of
252 FHR alone (0.32 μM) and in combination with Sbi-III-IV (1 μM). As shown in
253 Figure 3i and Supplementary Figure S3F, the presence of FHR-1, 2 or 5 increases
254 the C3b fluid phase half-life to different degrees, with FHR-5 showing the largest
255 increase in half-life. Most interestingly, the C3b half-life could be further
256 extended by the addition of Sbi-III-IV.
257
258 ***The Sbi-III-IV:C3d:FHR-1 tripartite complex forms a dimer in solution***
259 To investigate the structural characteristics of the Sbi-III-IV:C3d:FHR1
260 tripartite complex, we used small angle X-ray scattering (SAXS). The scattering
261 profile collected at an equimolar mixing ratio is shown in Figure 4 in log plot (a)
262 as well as Kratky plot (b). The featureless descend in the log plot and the plateau
263 in the latter is characteristic for scattering of particles that are, at least partially,
264 disordered.
265 The SAXS data and the overall parameters obtained (Supplementary Table
266 S2) suggest that the complex is largely dimeric but rather flexible in solution.
267 Quantitative flexibility analysis was performed using the ensemble optimisation
268 method EOM [32], which fits the experimental data using scattering computed
269 from conformational ensembles. Models with randomized linkers were
270 generated based on the known structures of FHR-$1_{1\text{-}2}$ (3zd2, [21]); $FH_{18\text{-}20}$ (3sw0,

271 [33]), containing the equivalent of FHR-1_3; FH_{19-20}:C3d complex (2xqw, [20]),
272 corresponding with FHR-1_{4-5}; and the Sbi-IV:C3d complex (2wy8, [34]). To
273 account for the dimerisation, P2 symmetry was applied, using the FHR-1_{1-2} dimer
274 interface as seen in the crystal structure (3zd2). The distributions of the overall
275 parameters in the selected structures compared with those of the original pool
276 (Figure 4c) suggests that the complex is rather flexible with a slight preference
277 for extended structures in solution. The subset of most typical models (and the
278 volume percentage of their contribution) shown in Figure 4c indicate that in
279 addition to the expected contact sites with C3d, Sbi-III domain appears to also
280 interact with FHR-1, corroborating the functional results described above. Figure
281 4d shows a schematic representation of the dimeric Sbi-III-IV:C3d:FHR-1
282 complex observed in solution.
283
284 ***K173A restricts the conformational freedom of Sbi domain III***
285 To examine the possible structural effects of the K173A substitution in Sbi
286 domain III, SAXS data was collected on the Sbi-III-IV(K173A):C3d complex and
287 compared to the wild-type Sbi-III-IV:C3d complex published previously [34]. The
288 experimental scattering pattern collected at 240 μM (~12 mg/ml) is presented
289 in Figure 4e and the structural parameters derived from this data are given in
290 Supplementary Table S2. The estimated molecular mass (MM) of the solute
291 agrees within the errors with the values predicted for a 1:1 complex (~15 kDa +
292 35 kDa). At lower concentration a decrease in the MM estimates is observed

293 which suggests that the complex slowly begins to dissociate. The previously
294 described wild-type Sbi-III-IV:C3d data on the other hand, suggests that at higher
295 concentrations, higher oligomeric species are present, thus, for the comparison
296 here, data collected at 0.6 mg/ml is shown. The faster descend of the wild-type
297 data, which translates to a larger Rg, suggests that rearrangements of the flexible
298 N-terminus lead to a more elongated particle (Rg wild-type= 32.8 Å) as
299 compared to K173A mutant (Rg K173A = 30.6 Å). This is in strong agreement
300 with the *switch*SENSE analysis of the C3d binding characteristics, which show a
301 reduced hydrodynamic diameter for K173A compared to WT (Table 2).
302 The *ab initio* low resolution models of the complex reconstructed from the
303 highest concentration data using DAMMIF [35] showed a large cone shaped
304 molecule with a volume of 124 nm^3 (Figure 4f). The resolution of the
305 reconstruction is estimated to be 29 +/- 2 Å [36]. The large base of the cone can
306 accommodate the crystal structure of Sbi-IV:C3d complex (2wy8) [34]. The extra
307 space at the tip of the cone would be sufficient to harbor the 60 N-terminal
308 residues comprising the Sbi-III domain. A more detailed modeling was
309 conducted with the program Coral [37], utilizing the available high-resolution
310 model of Sbi-IV:C3d and allowing for 60 additional beads to be added that mimic
311 the missing Sbi-III domain. Twenty independent Coral runs were performed
312 which all yielded models with a more or less structured N-terminal region,
313 suggesting that Sbi-III-IV(K173A) in complex with C3d is conformationally
314 restricted compared to wild-type Sbi-III-IV. This is further supported by the

315 narrow distributions obtained with EOM (Supplementary Figure S4B).
316 Surprisingly, whilst repeating these analyses using a proposed alternative
317 binding mode of the Sbi-IV:C3d complex (represented by 2wy7), where Sbi-IV is
318 seen bound at the convex face of C3d, the χ^2 value is greatly improved
319 (Supplementary Figure S4C). With this modeling approach a similar restricted
320 conformation is observed for the N-terminus of Sbi-III-IV(K173A). Further
321 studies are currently being conducted to further investigate the potential
322 physiological relevance of this alternative Sbi-IV:C3d binding mode.
323
324 ***A fusion construct of Sbi-III-IV with M. tuberculosis Ag85b activates the AP***
325 To test the potential of Sbi-III-IV to induce C3d opsonisation in a vaccine
326 setting, a recombinant construct was designed whereby Sbi-III-IV is fused to
327 *Mycobacterium* protein Ag85b (Figure 5a, and detailed in Supplementary Figure
328 S5A). Based on the SAXS structure of the Sbi-III-IV:C3d:FHR-1 tripartite complex,
329 revealing the importance of a flexible and extended conformation of Sbi domain
330 III, we decided to attach Ag85b at the C-terminus of Sbi domain IV and included a
331 long flexible linker between Sbi-IV and Ag85b to ensure accessibility and
332 flexibility of the functional domains. Expressed and purified fusion protein was
333 subsequently structurally and functionally characterized.
334 Circular dichroism analysis of the Sbi-III-IV-Ag85b fusion indicates that the
335 protein construct is folded and that the secondary structural elements of both
336 parent proteins have been preserved (Supplementary Figure S5B). SAXS data

337 obtained for the fusion protein demonstrate that both the Ag85b domain as well
338 as Sbi-IV domain are accessible (Figure 5b and Supplementary Figure S5C).

339 Functional activity of the Sbi-III-IV-Ag85b fusion construct was assessed
340 using an AP complement activity assays (WIESLAB, Euro Diagnostica), showing
341 strong C3 depletion activity (Supplementary Figure S5D), whilst Ag85b on its
342 own showed no complement activating properties. These results confirm that
343 the complement activating properties of Sbi III-IV are not impaired as part of the
344 fusion construct. The western blot analyses presented in Figure 5c and
345 Supplementary Figure S5E confirm these results, showing both C3 activation and
346 opsonisation by the Sbi-III-IV-Ag85b fusion construct when incubated with NHS.
347 Interestingly, C3 activation and consumption occur more rapidly with the fusion
348 construct when compared to Sbi-III-IV (Figure 1a and 1b) under the same
349 conditions. Whilst Sbi-III-IV shows opsonisation with a single molecule of C3b
350 (Figure 1b), the Sbi-III-IV-Ag85b fusion is opsonized by 2 molecules of C3b that
351 over time degrade to iC3b and C3d (Figure 5c and Supplementary Figure S5E).
352 Interestingly, opsonisation of Ag85b with C3 fragments also occurs when
353 co-incubated with Sbi-III-IV in NHS.
354

355 ***Sbi-III-IV acts as an adjuvant in mice when immunized with Ag85b***

356 Based on the ability of Sbi-III-IV to activate complement (Figures 1b, 1c
357 (human serum) and 6a (mouse serum)) and opsonise Ag85b with complement
358 C3 break down fragments (Figure 5c), we expected that this new fusion protein
359 when injected into mice would elicit a greater immune response to the

Sbi-III-IV-Ag85b fusion protein than Ag85b administered alone (in PBS). Indeed, wild-type C57bl/6 mice immunized I.P. (or I.V., data not shown) with Sbi-III-IV-Ag85b generated a greater than 4 fold increase in immune response initially and following the boost when compared to Ag85b alone (Figure 6b). Furthermore, when mice were immunized with a mixture of Sbi-III-IV and Ag85b (not fused together), this also resulted in a significantly improved immune response, corroborating the role of C3 fragment opsonisation of the antigen in this process (see Supplementary Figure S5E). Subsequent, studies using $C3^{-/-}$ and *Cr2*$^{-/-}$ mice clearly demonstrated that C3 and C3 breakdown fragment receptors (CR1 and CR2) were essential for this "adjuvant" function, respectively (Figure 6c). Overall, these data clearly suggest that complement AP dysregulation function of the Sbi-III-IV domain can be harnessed to improve immune responses through the coating of antigens with C3 breakdown fragments.

373 **Discussion:**

374 Previous work from our group [24] revealed that *Staphylococcus aureus*
375 immunomodulator Sbi binds complement component C3 within the thioester
376 domain of C3 or the C3dg portion of the molecule and resulted in futile
377 consumption of C3 via uncontrolled activation of the AP. In this study, we
378 endeavored to both understand the mechanism of action of Sbi-III-IV and
379 harness it; in order to develop pro-vaccines which would trigger natural
380 complement activation and thereby coat antigen surfaces with complement
381 component C3 degradation products, generate anaphylatoxins at the site of
382 immunisation and strongly enhance the immunogenicity of antigens (Figure 7d).

383 The seminal studies by Pepys *et al* [38], using C3 activating/depleting agents
384 including cobra venom factor and Zymosan, clearly demonstrated intact C3
385 function was important for the T-dependent response [38]. A molecular
386 mechanism explaining this effect was established by Fearon and colleagues [39]
387 supported by studies in both C3 [40] and *Cr2* (complement receptor type I and II)
388 knock-out mice [41]. Fearon *et al* exploited these findings and established that
389 multiple copies of C3d, in a linear trimer, could enhance antigen-specific
390 responses up to 10,000 fold [3]. However, the initial potential of trimeric C3d, as
391 a highly potent molecular adjuvant, has not been realized and the reason(s) for
392 this remain(s) unclear. One possible explanation is that the artificial linear
393 trimer structure fails to represent naturally opsonised antigen, and consequently
394 does not provide sufficient CR cross-linking or additional inflammatory signals

for the B cell (or APC) activation threshold to be reached. One possible approach to overcome this is attaching more C3d to test antigens, but that approach is also limited [42]. In the light of these and other findings [11, 13, 43], we considered that with understanding of the mode of action of Sbi-III-IV we might be able to develop a new complement activation based immune adjuvant.

The first clue to a mechanism for Sbi's ability to rapidly activate the AP came from monitoring Sbi-III-IV treated NHS in a time course using anti-C3 and anti-Sbi immuno-blotting. Here, we demonstrated that metastable C3b not only attaches covalently to serum proteins but also to Sbi-III-IV itself; as a transacylation target (Figure 1). This makes sense in the respect that Sbi's affinity to C3 obviously places it in close proximity to the site of complement turnover and we speculate that C3b deposited on Sbi-III-IV could help extend the fluid phase half-life of C3b, preventing FH and FI from binding and inactivating as normal, perhaps similar to covalent adducts of C3b with IgG [44, 45].

However, as we have shown previously, Sbi-III-IV also interacts with complement regulators FH and FHR-1, in addition to binding C3b and its degradation products, thereby forming tripartite complexes [26]. We next investigated whether Sbi-III-IV acts as a competitive antagonist of FH via the recruitment of FHR-1 and 5 into tripartite complexes and that FHR-1 can effectively displace FH from the tripartite complex. To this end, data from our systematic site-directed mutagenesis screen brought to light several Sbi mutants with complement activation defects (Figure 1, Supplementary Figure S1). For

instance, we demonstrated that an alanine substitution in Sbi domain III at position 173 resulted in a dramatic reduction in C3 consumption activity (Figure 1g). Notably, although a similar effect was observed with a previously identified mutation in domain IV with impaired C3d binding (R231A), K173A showed only slightly impaired C3d binding capacity (Table 1) suggesting a different mechanism. We therefore postulated that the K173A mutant would be ideal to elucidate the structural and functional role of Sbi domain III in the activation of complement and found that K173 in Sbi domain III was crucial for the recruitment of FHR-5 and that the K173A mutation only slightly affects FHR-1 binding (Figures 2 and 3). These findings implicate a direct role of Sbi domain III in the tripartite complex formation with these FHRs and that this likely occurs via interactions with the C-terminal SCR domains that share sequence identity with FH_{19-20}. We confirm this by showing that increasing concentrations of recombinant FHR-1, FHR-2, FHR-5 and FH_{19-20} in serum indeed potentiate Sbi-III-IV mediated C3 consumption, whilst the N-terminal SCRs ($FHR\text{-}1_{1-2}$) fails to do this (Figure 3).

We also observed that Sbi greatly enhances the binding of FHRs to C3b, thereby antagonizing FH activity, as shown by the C3 convertase decay accelerating activity (DAA) assay (Figure 3 g and h). These results imply that the FHR-1 or FHR-5 containing tripartite complexes can protect the AP C3 convertase, aiding the consumption of C3. These findings further enhance the notion that the FHR family has diversified AP de-regulatory functions, where

439 FHR-1 seems more efficient in counteracting the DAA of FH, whilst in contrast
440 FHR-5 potently antagonizes the cofactor activity (CA) of FH. The observed
441 Sbi-III-IV mediated shift in the complement regulatory balance towards C3
442 activation could potentially be further enhanced by the formation of
443 homo/heterodimeric forms of FHR-1 with itself and with other FHRs (FHR-2 and
444 FHR-5) [12]. These data link to an ongoing evolutionary 'arms race' where FH
445 was initially hijacked by *S. aureus* to protect it from complement [46] and then
446 FHRs (devoid of intrinsic complement regulatory activity) were
447 evolved/deployed by the host to compete with FH on that surface and restore
448 complement opsonisation of the pathogen [22]. Perhaps the release/secretion of
449 Sbi from *S. aureus* is a more recent event in this arms race with the host, which
450 takes the C3b/C3 convertase binding potential away from the bacterial surface
451 and leads to local rapid fluid phase consumption of complement, i.e. local
452 decomplementation and bacterial survival/propagation. Our understanding of
453 the role and complexity of FHRs in immune evasion strategies is still in its
454 infancy [46], but this study underlines the potency of another strategy in this
455 process.

456 Using FHR-1 as a 'model' dimerization domain containing FHR, structural
457 analysis of the Sbi-III-IV:C3d:FHR-1 tripartite complex, using SAXS, indeed
458 suggests the formation of a dimer mediated by FHR-1 domain 1 and 2 and
459 provides details of the role of the extended unfolded nature of domain III in the
460 binding of FHR-1 (Figure 4). The molecular basis of the preferential binding of

461 FHR-1 over FH cannot easily be explained on the basis of differences in amino
462 acid sequence between the two complement regulators, since their C3d binding
463 regions (SCR 4-5 of FHR-1 and SCR 19-20 of FH) share 99% sequence identity.
464 However, our SAXS analyses, and binding studies using C3d(g) or iC3b as ligands
465 (Figures 3 and 4), indicate that the C-terminal regions of FHR proteins are
466 readily exposed, unlike those of FH that exist in a "latent" conformation with the
467 C-terminal part of the protein folded back and partially blocked [47-50]. The
468 dimeric physiological state of FHR-1 and the other FHRs tested in this study is
469 also likely to enhance their ability, due to increased avidity, to assemble a
470 tripartite complex.
471
472 Analysis of the hydrodynamic volume of the Sbi-III-IV:C3d complex using
473 *switch*SENSE highlighted a significant contraction of the normally extended
474 conformation Sbi-III-IV structure [34] caused by the K173A substitution in
475 domain III (Table 2). SAXS analysis confirms these findings, showing a partially
476 kinked N-terminal structure of domain III in K173A with reduced conformational
477 freedom (Figure 4e-g). The contraction of the Sbi-III-IV structure caused by the
478 K173A substitution suggests that the normally flexible and extended
479 conformation of domain III plays an important role in the recruitment of FHRs,
480 especially FHR-5 into the tripartite complex after the initial interaction between
481 Sbi-IV and C3b. Previous structural analyses of the Sbi's domain III, using NMR,
482 revealed that this domain is indeed natively unfolded [51].

Based on the structural and functional information described here we decided to construct a Sbi-III-IV-Ag85b fusion construct that could be used to test its effect on the immune response against this model antigen *in vivo*. We chose *Mycobacterium tuberculosis* Ag85b, a fibronectin-binding protein with mycolyltransferase activity [52], because it is known to be immunogenic and previously suggested as a vaccine candidate [53]. Indeed, there is evidence that Ag85b can elicit both humoral and cellular immune reactions in patients with TB, but there is conflicting evidence of its efficacy as a vaccine [54, 55], suggesting adjuvants may improve its overall immunogenicity. This target also gives scope to allow further testing in animal models of disease [56]. Structural analysis, using Circular Dichroism and SAXS confirmed that secondary structural elements of both parent proteins have been preserved in the fusion protein construct and that the crucial functional Sbi domains are accessible for interactions with complement (Figure 5 and Supporting Figure S5). We also show that the Sbi-III-IV-Ag85b fusion construct can induce AP activation and is opsonized with C3 breakdown products (Figure 5c).

With AP activation in human and mouse serum confirmed (Figures 5 and 6), we opted to use straightforward immune response, IgG titre, analysis to demonstrate the potential of Sbi-III-IV to trigger complement *in vivo* and act as a vaccine adjuvant in a mouse model, in a similar manner to many previous studies [57]. Our data herein firstly indicates that Sbi-III-IV can activate mouse

505 complement in an analogous manner to that of the human complement system.
506 This obviously allows direct analysis of these pro-vaccine compounds in both
507 mouse and human model systems (a huge advantage to previous C3d based
508 adjuvants) [13], indeed Sbi-III-IV has acted as a C3 activator in all species tested
509 thus far (data not shown). As predicted from the *in vitro* work, the opsonisation
510 of fusion proteins or co-immunised antigen by mouse complement breakdown
511 fragments results in a significant increase in the immunogenicity of Ag85b, with
512 increased IgG titres noted in the presence of fused or co-immunised Ag85b
513 (Figure 6). The adjuvant function both increased the intensity of the response
514 and the rate of the response when compared to Ag85b immunized alone. We will
515 need to further explore the potency of this response to that of common adjuvants
516 and with a mix of target antigens to fully assess the utility of Sbi-III-IV as a
517 universal vaccine adjuvant. For instance, comparison of the action of Sbi-III-IV to
518 the Glaxo-Smith-Kline's adjuvant systems, particularly AS01 [58], or to MF59 [59]
519 may be of key interest and recent approaches may provide ideal pre-clinical
520 model systems to facilitate this [60, 61] before progression to clinical studies.
521 The work is ongoing but the data herein demonstrate the initial proof of concept.
522
523 In summary, we have demonstrated that Sbi-III-IV triggers consumption of
524 complement component C3 via activation of the alternative complement
525 pathway, by acting as a competitive antagonist of FH via the recruitment of FHRs
526 into dimeric tripartite complexes that can protect C3b bound to Sbi (Figure 6d).

It is likely this provides a stable nidus for alternative pathway mediated C3 convertase generation, i.e. local fluid phase C3bBb generation that overwhelms any local complement regulators, providing the potential for bystander lysis or opsonisation of surfaces. Our ability to harness this potential, targeting complement opsonisation to the surface of an antigen (in this case from *Mycobacterium)* and therefore use Sbi-III-IV as a vaccine adjuvant clearly demonstrates Sbi-III-IV has great potential for use with a range of antigens across multiple species, including humans, although more work remains to make that a reality.

Materials and Methods

Proteins, antibodies and sera

Factor H (FH), C3b, factor B (FB), factor D (FD), factor I (FI), properdin (FP), FI-depleted serum, goat anti-human C3 polyserum and goat anti-human FB polyserum were purchased from Complement Technologies (Tyler, TX). FHR-1_{1-2}, FHR-1, -2 and -5 used in the tripartite complex reconstruction and binding competition assay were produced using Chinese Hamster ovary cell culture (as previously described [62]). Horse radish peroxidase (HRP)-conjugated rabbit anti-goat immunoglobulin polyserum and HRP-conjugated Streptavidin were acquired from Sigma Aldrich. HRP-conjugated goat anti-rabbit immunoglobulin G (Thermo Fisher, catalog no. 815-968-0747), HRP-conjugated rabbit anti-mouse immunoglobulin G (Thermo Fisher, catalog no. 31452) and biotin-conjugated FH monoclonal antibody OX24 (catalog no. MA5-17735) were purchased from Thermo Fisher Scientific. The goat anti-human FH polyclonal serum (catalog no. 341276-1ml) that was previously used to detect human FH and FHR-1 was purchased from Merck Millipore. Human C3 was purified from mixed pool citrated human plasma (TCS Bioscience, PR100) using polyethylene glycol 4000 precipitation, anion and cation exchange chromatography as previously described [63]. A pET15b-C3d construct was acquired from Prof. David E. Isenman and transformed into *Escherichia coli* (*E. coli*) stain BL21 (DE3), recombinant C3d was then expressed and purified using a previously described

558 protocol [64]. Lyophilized normal human serum (NHS) was purchased from Euro
559 Diagnostica (catalog no. PC300). Additional proteins and antibodies are
560 described in the specific experimental sections.

561

562 *Sbi-III-IV constructs*

563 The expression and purification of the N-terminally 6×His tagged recombinant
564 Sbi-III-IV from a pQE30:*sbi-III-IV* construct were described previously [24].

565

566 *Sbi-III-IV mutagenesis*

567 Mutations in the Sbi-III-IV sequence were introduced using the QuikChange II XL
568 site-directed mutagenesis kit (Agilent Technologies), the primers used are listed
569 in Supplementary Table S1. The mutated pQE30:*sbi-III-IV* plasmids were
570 sequenced to confirm the success of the mutagenesis. SDS-PAGE profiles of all
571 the Sbi-III-IV mutant proteins used in this study are shown in Supplementary
572 Figure S1.

573

574 *Sbi-III-IV induced C3 consumption assay*

575 Lyophilized NHS was re-suspended in chilled dH_2O to a 2× concentration. Equal
576 volumes of 2×NHS and Sbi (10 µM) were combined. Sbi treated sera were then
577 incubated in a thermocycler at 37°C for 30 min. Treated serum samples were
578 collected at time intervals, 0.5 µl of serum was loaded on an SDS-PAGE gel
579 analyzed under reducing condition. The proteins were Western blotted, and the

580 blots were probed with anti-C3d, anti-Sbi, anti-C3a or anti-factor B antibodies.

581

582 A hemolytic assay was modified from a previously published procedure [65] to
583 measure Sbi induced consumption of C3. Briefly, rabbit erythrocytes (TCS
584 Bioscience) were resuspended in GVB buffer (5 mM veronal, 145 mM NaCl, 10
585 µM EDTA, 0.1 % (w/v) gelatin) by washing three times via centrifugation at 600
586 *g* for 6 mins. The concentration of rabbit red cells to be used in each experiment
587 was determined by adding a stock of 5 µl of erythrocytes to 245 µl of water to
588 give complete lysis and then re-adjusting cell concentration until an optical
589 density reading of 0.7 (A_{405}) was reached. Lysis experiments were conducted in
590 two steps, first, 15 µl of NHS, 5 µl of Mg^{+}-EGTA (70 mM $MgCl_2$ and 100 mM
591 EGTA), 20 µl of protein in E2 buffer was mixed and pre-incubated at 37 °C for 30
592 mins. Subsequently, 5 µl of rabbit erythrocyte was added and incubated for an
593 additional 30 mins at 37 °C. At the end of the incubation, 150 µl of quenching
594 buffer (GVB supplemented with 10 mM EDTA) was added. The cells were
595 pelleted by centrifugation at 1500*g* for 10 min, and absorbance (A_{405}) of 100 µl
596 of supernatant measured. Post-consumption lysis percentage was calculated as
597 $100\times((A_{405}$ test sample-A_{405} 0% control)/(A_{405} 100%-A_{405} 0% control)).

598

599 *In vitro complement activation using Sbi III/IV-Ag85b in mouse serum*

600 Mouse serum was collected from male *Cr2*$^{-/-}$ mice by cardiac puncture and
601 allowed to clot fully on ice for 4 hours followed by separation of serum by

602 centrifugation at 2000g in a refrigerated centrifuge. Serum was then mixed with
603 Sbi III/IV or Sbi III/IV-Ag85b, ensuring that the amount of Sbi III/IV in each
604 preparation was equivalent. The reaction was stopped at 0, 30, 60 and 120
605 minutes, by the addition of reducing sample buffer, boiled for 5 min and analysed
606 on a 10% SDS-PAGE gel. After transfer to nitrocellulose the blots were probed
607 with Rabbit anti-C3d (1/1000, DAKO, A0063) and Goat anti-Rabbit-HRPO
608 (1/2000, 111-035-046-JIR, Stratech), developed with ECL substrate (Pierce) and
609 exposed to X-Ray film for 2 min.
610
611 *switchSENSE kinetic analysis*
612 A switchSENSE DRX 2400 instrument (Dynamic Biosensors) was used to
613 characterize the binding kinetics and protein size changes based on *switch*SENSE
614 technology [66, 67]. Purified Sbi-III-IV-cys, K173A, R231A and their ligand C3d
615 were sent to Dynamic Biosensor's protein analyzing facility for binding kinetic
616 and hydrodynamic diameter analysis. In the case of a protein binding event,
617 based on the real-time measurements of the switching dynamics in a range of
618 ligand concentrations, binding rate constants (k_{ON} and k_{OFF}) and dissociation
619 constants (K_D) can be analysed [67]. Alternatively, under saturated binding
620 conditions, the switching dynamic of the protein (or protein complex) can be
621 compared with the switching dynamics of bare DNA and with a biophysical
622 model with which the size of the immobilized protein (or protein complex) can
623 be determined. For determination of Sbi-III-IV:C3d binding kinetic parameters,

130 nM, 100 nM, 70 nM and 40 nM of C3d were applied sequentially onto the Sbi-III-IV immobilized microchip. All Sbi:C3d complexes' hydrodynamic diameters were estimated at a C3d concentration of 130 nM.

Fluorometric assay

Fluorometric C3b breakdown assay was performed using a black 96 well microplate (Thermofisher, M33089) in a TECAN Spark 20M temperature-controlled fluorescence plate reader. Excitation was at 386 nm and emission was recorded at 475 nm with a 20-nm bandwidth. The control C3b breakdown rate, performed in PBS, contained 100 µl of 1 µM C3b, 160 nM FH, 17 nM of FI and 10 µM ANS, and was scanned every 5 *s* for 15 min. To study the interruption of C3b breakdown, 32 nM of FHR was either added alone or in combination with 1 µM of Sbi-III-IV. Data were collected at 25°C, normalized by Excel using the equation "Percentage of C3b=((F_X-(F_{15min}))/(F_{15min}-F_{0min}))*100" and plotted by Graphpad Prism.

Small angle X-ray scattering

Synchrotron radiation X-ray scattering from solutions of the Sbi-III-IV:C3d:FHR-1 tripartite complex, the Sbi-III-IV(K173A):C3d complex, and the Sbi-III-IV-Ag85b fusion protein were collected at the EMBL P12 beamline of the storage ring PETRA III (DESY, Hamburg, Germany). Images were collected using a photon counting Pilatus-2M detector and a sample to detector distance of

646 3.1 m and a wavelength (λ) of 0.12 nm covering the range of momentum transfer
647 (s) 0.1 < s< 4.5 nm^{-1}; with $s=4\pi\sin\theta/\lambda$. Different solute concentrations were
648 measured using a continuous flow cell capillary. To monitor radiation damage,
649 20 successive 50 ms exposures were compared and frames displaying significant
650 alterations were discarded. The data were normalized to intensity of the
651 transmitted beam and radially averaged; the scattering of the buffer was
652 subtracted, and the different curves were scaled for solute concentration. The
653 forward scattering I(0), the radius of gyration (Rg) along with the probability
654 distribution of the particle (p(r)) and the maximal dimension (D_{max}) were
655 computed using the automated SAXS data analysis pipeline SASFLOW [68].

656 For the Sbi-III-IV-Ag85b fusion protein data quality was improved with
657 SEC-SAXS mode and the parallel analysis of light scattering data in a similar
658 manner as described in Gräwert *et al*. [69]. Frames comprising solely the
659 monomeric version of the fusion protein were averaged and used for further
660 processing after background subtraction.

661 The molecular masses (MM) were evaluated by comparison of the forward
662 scattering with that from a reference solution of BSA and based on the Porod
663 volumes of the constructs. With SAXS, the former estimation of MM is within an
664 error of 10%, provided the sample and standard concentrate are determined
665 accurately. DAMMIF was used to compute the *ab initio* shape models. For this, 10
666 independent models fitting the experimental scattering curves were generated
667 and compared to each other. More detailed modelling was obtained with Coral.

668 Here, existing partial crystal structure of the Sbi-IV:C3d complex was extended
669 with 60 additional beads placed at the N-terminus of Sbi-IV to mimic the missing
670 Sbi-III domain. Here too, 10 independent runs were performed, and the degree of
671 variation addressed. Further analysis of the flexibility of the samples was
672 addressed with Ensemble Optimization Method (EOM). For this, ensembles of
673 models with variable conformations are selected from a pool of randomly
674 generated models such that the scattering from the ensemble fits the
675 experimental data, and the distributions of the overall parameters (e.g. D_{max}) in
676 the selected pool are compared to the original pool.

677 The proteins in the Sbi-III-IV:C3d:FHR-1 tripartite complex were combined
678 1:1:1 at a concentration of 45 μM. The Sbi-III-IV(K173A):C3d complex were
679 formed at a 1:1 ratio at 240 μM (12 mg/ml). PDB structure 2wy8 (Sbi-IV:C3d
680 complex) was used to model the complex using and compared with SAXS data
681 previously recorded [34]. The Sbi-III-IV-Ag85b fusion protein was provided at 29,
682 72 and 145 μM concentrations (1.45, 3.6 and 7.2 mg/ml, respectively). The
683 samples were dialysed against PBS, which was also used for background
684 subtraction. From all samples concentration series were measured to exclude
685 any concentration dependent alterations.

686

687 *Surface Plasmon Resonance*

688 Tripartite complexes were analyzed by surface plasmon resonance (SPR)
689 technology using a Biacore S200 (GE Healthcare). All experiments were

conducted at 25°C on CM5 chips, using HBST (10 mM HEPES, 150 mM NaCl, and 0.005% Tween 20, pH 7.4) as running buffer, which was optionally supplemented with 1mM of $MgCl_2$ ($HBST^+$) to be compatible with AP amplification condition. On the chip surface 800 RU of C3b was opsonized via AP C3 convertase through a method described before [70, 71]. The iC3b surface was produced by injecting of repetitive cycles of FH and FI across a C3b opsonized surface, the completeness of the conversion was confirmed by the inability of FB binding. A separate chip surface was made by amine coupling 600 RU of recombinant C3d (CompTech, USA). In all SPR experiments, response differences were derived using the signal from a flow cell to subtract the parallel reading from a reference flow cell that blocked with carbodiimide, *N*-hydroxysuccinimide and ethanolamine. Analytes were injected in duplicate (at 30 µl/min for 200 *s*) followed by running buffer for 300 *s* and a regeneration phase involving injection of regeneration buffer (10 mM sodium acetate, 1 M NaCl pH 4.0) for 60 *s*. To analyze Sbi-III-IV binding and the assembly of tripartite complex, concentration series of Sbi-III-IV WT or K173A were flowed cross separately or co-injected with FH, FHR-1, FHR-2, FHR-5 or FH_{19-20} at a fixed concentration (100, 12.5, 20, 25 or 20 nM respectively).

The C3 convertase DAA assay was performed on a CM5 chip amine coupled with 500 RU C3b, using $HBST^+$ as running buffer throughout. A mixture of analytes for building C3 convertase were flowed across, including FB and FD in addition to

712 various FH reagent combinations (FH or FH and FHR-1 or FH, FHR-1 and -5). The
713 various FH reagents combinations were also flow across separately in order to
714 derive the sensorgram for C3 convertase. To examining Sbi bound C3 convertase,
715 2 μM of wild-type Sbi-III-IV was added to the mixture of analytes for building C3
716 convertase. The various FH reagent combinations spiked with Sbi were flowed
717 across separately in order to derive the sensorgram for Sbi bound C3 convertase.
718 Each injection cycle includes Injection of the C3 convertase mixture for 200-300
719 *s*, followed by running buffer for 300-400 *s* and two consecutive 60 *s*
720 regeneration phases.
721
722 *FH/FHR-1 Competition assay*
723 C3b was diluted in carbonate buffer (pH 9.5) and coated on to wells of a Nunc
724 MaxiSorp plate (0.25 μg/well) for 16 h at 4°C. The wells were blocked with PBST
725 (PBS with 0.1% Tween 20) supplemented with and 2% BSA for 1 h at 37 °C, and
726 then washed with PBST buffer. Doubly diluted concentration series (9-600 nM)
727 of FHRs, FH_{19-20}, $FHR\text{-}1_{1-2}$ in PBST-2% BSA were then added to the wells,
728 together with a constant concentration of FH (25 nM) and Sbi-III-IV (1000 nM).
729 The plate was incubated for 1 h at 37 °C, then washed with PBST. 50 μl of
730 monoclonal anti-FH antibody OX-24 (specific to the FH SCR domain 5) diluted
731 with PBS-2% BSA (0.6 μg/ml) was added to the wells and the plate incubated for
732 a further 1 h. The wells were washed with PBST, and 50 μl sheep anti-mouse IgG
733 (1:5000 dilution in PBST-2% BSA) was added to the wells for 1 h at 37 °C. The

734 wells were washed again and the conjugate was detected using TMB ELISA
735 substrate solution, which was added to the wells for 5 min. The colour reaction
736 was stopped by 10% H_2SO_4 and the plate was read at A_{450} using a plate reader.
737
738 *Design and purification of the Sbi-III-IV-Ag85b fusion construct*
739 The DNA sequence coding for Sbi-III-IV ($sbi_{448\text{-}798}$) was fused to the 5' end of the
740 DNA sequence for Ag85b ($ag85b_{121\text{-}975}$) via a linker region of 84 bp
741 (Supplementary Figure S6). The fusion gene was commercially synthesized and
742 ligated into the pET15b vector, containing an ampicillin resistance cassette and a
743 T7 promoter. The pET15b:*sbi-III-IV-ag85b* plasmid was verified using
744 sequencing, and the resulting construct encoded an N-terminally his-tagged
745 Sbi-III-IV-Ag85b protein. *E. coli* BL21 (DE3) cells harbouring the
746 pET15b:*sbi-III-IV-ag85b* plasmid were grown in LB broth supplemented with
747 100 µg/ml ampicillin to an A_{600} = 0.4-0.6. Protein expression was induced with
748 0.5 mM IPTG and by incubating the cells at 17°C for 16 h. Bacteria were
749 harvested, lysed using sonication (80% amplitude, for six 10 s bursts) in the
750 presence of protease inhibitor cocktail (set VII-Calbiochem, Merck), and the
751 protein initially purified using nickel-affinity chromatography (His-Trap column,
752 GE Healthcare) with a gradient of 0-0.5 M imidazole in 50 mM Tris, 150 mM NaCl,
753 pH 7.4. It was further purified using size-exclusion chromatography (Hi-Load
754 16/60 Superdex S200 column, GE Healthcare) equilibrated in 20 mM Tris, 150
755 mM NaCl, pH 7.4. Fractions containing protein were pooled and concentrated.

Protein concentration was measured at A_{280}.

Analysis of Sbi-III-IV-Ag85b fusion protein AP complement activity

Alternative pathway (AP) activity of Sbi III-IV-Ag85b-treated NHS samples was analysed using the ELISA-based WIESLAB® (Euro Diagnostica) complement system AP assay. Sbi-III-IV-Ag85b was mixed with normal human serum (NHS) at a 1:1 volume ratio and incubated for 30 min at 37 °C in a thermal cycler. Treated serum was then diluted with AP diluent (blocking the activation of the other two complement pathways) by 1 in 20. From this point the manufacturer's instructions were followed. A blank (AP diluent), positive control (NHS) and negative control (heat-inactivated NHS) were also recorded. Complement activation was converted to residual AP activity (%) using the equation: (sample - negative control)/(positive control - negative control) x 100.

C3 fragment deposition on Sbi-III-IV-Ag85b fusion protein

The method used is similar to that described for WT Sbi-III-IV. Lyophilised NHS (Euro Diagnostica) was re-suspended in chilled dH_2O. Sbi-III-IV-Ag85b (100 μM) was mixed with NHS in a 1:1 ratio, and incubated for 1 h at 37 °C in a thermocycler. Samples were taken at regular intervals (0, 5, 15, 30, 60 min), and separated by SDS-PAGE followed by Western blot analysis using either rabbit anti-Sbi (1.5: 5000 dilution), rabbit anti-C3d (1.5:5000 dilution) or mouse anti-Ag85b (1:1000 dilution) polyclonal antibodies and detected using

778 HRP-conjugated secondary antibodies (1:2500 goat anti rabbit or 1:1000 goat
779 anti mouse). NHS-only was used as a negative control.
780
781 *Measurement of immune response to Sbi-III-IV-Ag85b fusion protein*
782 Eight week old male mice (wild-type C57bl/6, $C3^{-/-}$ and $Cr2^{-/-}$) were bled by tail
783 vein venesection at day -2. Mice were then immunized at day 0 with molar
784 equivalent doses of Ag85b alone (2μg), Sbi-III-IV-Ag85b (fusion protein),
785 Sbi-III-IV alone or a mixture of Sbi-III-IV and Ag85b, as appropriate. Mice were
786 then bled weekly thereafter and plasma stored at -80°C until required for batch
787 analysis. Mice were boosted at day 28 and sacrificed at day 42.
788 For analysis of IgG response to Ag85b by ELISA, 96 well plates (NUNC maxisorb)
789 were coated with 1 μg/ml Ag85b (Abcam, UK) or 1.35 μg/ml Sbi III/IV-Ag85b in
790 carbonate buffer at 50 μl per well and incubated at 4°C for 16 h. Plates were
791 washed with 0.01% PBS-Tween and a 1% BSA blocking solution was applied for
792 1 h at 20°C. Serum samples were diluted to 1/50 or 1/100 in 0.01% PBS-Tween,
793 added at 50 μl per well and incubated for 1 h at 20°C. Plates were washed and
794 secondary antibody (sheep anti mouse IgG-HRPO, 515-035-071-JIR, Stratech, UK)
795 was added at 1/100 dilution, 50 μl per well and incubated for 1 h at 20°C. TMB
796 substrate (50 μl per well) was added and allowed to develop for 6 min. The
797 reaction was stopped by the addition of 100 μl 10% H_2SO_4 per well and plates
798 were read at A_{450}. A mouse monoclonal anti-Ag85b (Abcam, ab43019) used as a
799 positive control. The mean absorbance ± SEM of each mouse group is shown.

800 Data for each mouse, at time 0, has been normalized to the day 0 average

801 reactivity to Ag85b in all mice screened.

Acknowledgements

This research was funded by the Biotechnology and Biological Sciences Research Council (BBSRC Follow On Fund BB/N022165/1, awarded to JvdE and KJM). AAW was supported by a PhD scholarship granted Raoul and Catherine Hughes and the University of Bath Alumni. KJM, HD and RW were also supported by the MRC and Newcastle University's Confidence in Concept funding. AS thanks the Royal Society URF and Alumni Fund at the University of Bath for funding. MAG was supported by the EMBL interdisciplinary Postdoc Programme under Marie Curie COFUND Actions as well as the Horizon 2020 programme of the European Union, iNEXT (H2020 Grant # 653706).

Author Contributions

JvdE, AGW and KJM conceived the idea of the project. YY, KJM and JvdE designed the experiments. YY, CRB, AAW, RK and JP performed and analysed the experiments. KW and WK conducted and analysed the *switch*SENSE experiments. MAG and DIS conducted SAXS experiments and oversaw the structural analysis. RK, JP and KJM conducted the *in vivo* experiments. AS and AW significantly contributed to the discussions about the overall project. YY, CRB, KJM and JvdE wrote and edited the manuscript, with significant contributions from AAW, MAG and DIS.

Competing Financial Interests

824 KW and WK are employed by Dynamic Biosensors GmbH

825 KJM is a member of the scientific advisory board of Gemini Therapeutics, Inc,
826 Cambridge, Massachusetts, USA.

827

828 **Data availability**

829 All data generated or analysed during this study are included in this published
830 article (and its supplementary information files).

831

References

1. Green, T.D., et al., *C3d enhancement of neutralizing antibodies to measles hemagglutinin.* Vaccine, 2001. **20**(1-2): p. 242-8.
2. Ross, G.D., *Regulation of the adhesion versus cytotoxic functions of the Mac-1/CR3/alphaMbeta2-integrin glycoprotein.* Crit Rev Immunol, 2000. **20**(3): p. 197-222.
3. Dempsey, P.W., et al., *C3d of complement as a molecular adjuvant: bridging innate and acquired immunity.* Science, 1996. **271**(5247): p. 348-50.
4. Fang, Y., et al., *Expression of complement receptors 1 and 2 on follicular dendritic cells is necessary for the generation of a strong antigen-specific IgG response.* J Immunol, 1998. **160**(11): p. 5273-9.
5. Carroll, M.C. and D.E. Isenman, *Regulation of humoral immunity by complement.* Immunity, 2012. **37**(2): p. 199-207.
6. Roozendaal, R. and M.C. Carroll, *Complement receptors CD21 and CD35 in humoral immunity.* Immunol Rev, 2007. **219**: p. 157-66.
7. Popi, A.F., I.M. Longo-Maugeri, and M. Mariano, *An Overview of B-1 Cells as Antigen-Presenting Cells.* Frontiers in immunology, 2016. **7**: p. 138.
8. Chan, O.T., M.P. Madaio, and M.J. Shlomchik, *B cells are required for lupus nephritis in the polygenic, Fas-intact MRL model of systemic autoimmunity.* J Immunol, 1999. **163**(7): p. 3592-6.
9. Ron, Y., et al., *Defective induction of antigen-reactive proliferating T cells in B cell-deprived mice.* Eur J Immunol, 1981. **11**(12): p. 964-8.
10. Ron, Y., et al., *Defective induction of antigen-reactive proliferating T cells in B cell-deprived mice. II. Anti-mu treatment affects the initiation and recruitment of T cells.* Eur J Immunol, 1983. **13**(2): p. 167-71.
11. De Groot, A.S., et al., *C3d adjuvant effects are mediated through the activation of C3d-specific autoreactive T cells.* Immunol Cell Biol, 2015. **93**(2): p. 189-97.
12. Carter, R.H. and D.T. Fearon, *Polymeric C3dg primes human B lymphocytes for proliferation induced by anti-IgM.* J Immunol, 1989. **143**(6): p. 1755-60.
13. He, Y.G., et al., *A novel C3d-containing oligomeric vaccine provides insight into the viability of testing human C3d-based vaccines in mice.* Immunobiology, 2018. **223**(1): p. 125-134.
14. van den Elsen, J.M. and D.E. Isenman, *A crystal structure of the complex between human complement receptor 2 and its ligand C3d.* Science, 2011. **332**(6029): p. 608-11.
15. Janssen, B.J., et al., *Structures of complement component C3 provide insights into the function and evolution of immunity.* Nature, 2005. **437**(7058): p. 505-11.
16. Janssen, B.J., et al., *Structure of C3b reveals conformational changes that underlie complement activity.* Nature, 2006. **444**(7116): p. 213-6.
17. Forneris, F., et al., *Structures of C3b in complex with factors B and D give*

insight into complement convertase formation. Science, 2010. **330**(6012): p. 1816-20.

18. Wu, J., et al., *Structure of complement fragment C3b-factor H and implications for host protection by complement regulators.* Nat Immunol, 2009. **10**(7): p. 728-33.
19. Morgan, H.P., et al., *Structural basis for engagement by complement factor H of C3b on a self surface.* Nat Struct Mol Biol, 2011. **18**(4): p. 463-70.
20. Kajander, T., et al., *Dual interaction of factor H with C3d and glycosaminoglycans in host-nonhost discrimination by complement.* Proc Natl Acad Sci U S A, 2011. **108**(7): p. 2897-902.
21. Goicoechea de Jorge, E., et al., *Dimerization of complement factor H-related proteins modulates complement activation in vivo.* Proceedings of the National Academy of Sciences, 2013. **110**(12): p. 4685-4690.
22. Jozsi, M., et al., *Factor H-related proteins determine complement-activating surfaces.* Trends Immunol, 2015. **36**(6): p. 374-84.
23. Xue, X., et al., *Regulator-dependent mechanisms of C3b processing by factor I allow differentiation of immune responses.* Nat Struct Mol Biol, 2017. **24**(8): p. 643-651.
24. Burman, J.D., et al., *Interaction of human complement with Sbi, a staphylococcal immunoglobulin-binding protein indications of a novel mechanism of complement evasion by Staphylococcus aureus.* Journal of Biological Chemistry, 2008. **283**(25): p. 17579-17593.
25. Smith, E.J., et al., *The immune evasion protein Sbi of Staphylococcus aureus occurs both extracellularly and anchored to the cell envelope by binding lipoteichoic acid.* Molecular Microbiology, 2012. **83**(4): p. 789-804.
26. Haupt, K., et al., *The Staphylococcus aureus Protein Sbi Acts as a Complement Inhibitor and Forms a Tripartite Complex with Host Complement Factor H and C3b.* Plos Pathogens, 2008. **4**(12).
27. Csincsi, A.I., et al., *Factor H-related protein 5 interacts with pentraxin 3 and the extracellular matrix and modulates complement activation.* J Immunol, 2015. **194**(10): p. 4963-73.
28. van Beek, A.E., et al., *Factor H-Related (FHR)-1 and FHR-2 Form Homo- and Heterodimers, while FHR-5 Circulates Only As Homodimer in Human Plasma.* Front Immunol, 2017. **8**: p. 1328.
29. Isenman, D.E., et al., *Nucleophilic modification of human complement protein C3: correlation of conformational changes with acquisition of C3b-like functional properties.* Biochemistry, 1981. **20**(15): p. 4458-67.
30. Pangburn, M.K. and H.J. Muller-Eberhard, *Kinetic and thermodynamic analysis of the control of C3b by the complement regulatory proteins factors H and I.* Biochemistry, 1983. **22**(1): p. 178-85.
31. McRae, J.L., et al., *Human factor H-related protein 5 has cofactor activity, inhibits C3 convertase activity, binds heparin and C-reactive protein, and associates with lipoprotein.* Journal of immunology (Baltimore, Md : 1950), 2005. **174**(10): p. 6250-6.

32. Tria, G., et al., *Advanced ensemble modelling of flexible macromolecules using X-ray solution scattering.* IUCrJ, 2015. **2**(Pt 2): p. 207-17.
33. Morgan, H.P., et al., *Structural analysis of the C-terminal region (modules 18-20) of complement regulator factor H (FH).* PLoS One, 2012. **7**(2): p. e32187.
34. Clark, E.A., et al., *A structural basis for Staphylococcal complement subversion: X-ray structure of the complement-binding domain of Staphylococcus aureus protein Sbi in complex with ligand C3d.* Molecular Immunology, 2011. **48**(4): p. 452-462.
35. Franke, D. and D.I. Svergun, *DAMMIF, a program for rapid ab-initio shape determination in small-angle scattering.* Journal of Applied Crystallography, 2009. **42**: p. 342-346.
36. Tuukkanen, A.T., G.J. Kleywegt, and D.I. Svergun, *Resolution of ab initio shapes determined from small-angle scattering.* IUCrJ, 2016. **3**(Pt 6): p. 440-447.
37. Petoukhov, M.V., et al., *New developments in the ATSAS program package for small-angle scattering data analysis.* Journal of Applied Crystallography, 2012. **45**: p. 342-350.
38. Pepys, M.B., *Role of complement in induction of antibody production in vivo. Effect of cobra factor and other C3-reactive agents on thymus-dependent and thymus-independent antibody responses.* J Exp Med, 1974. **140**(1): p. 126-45.
39. Fearon, D.T. and R.H. Carter, *The CD19/CR2/TAPA-1 complex of B lymphocytes: linking natural to acquired immunity.* Annu Rev Immunol, 1995. **13**: p. 127-49.
40. Wessels, M.R., et al., *Studies of group B streptococcal infection in mice deficient in complement component C3 or C4 demonstrate an essential role for complement in both innate and acquired immunity.* Proc Natl Acad Sci U S A, 1995. **92**(25): p. 11490-4.
41. Ahearn, J.M., et al., *Disruption of the Cr2 locus results in a reduction in B-1a cells and in an impaired B cell response to T-dependent antigen.* Immunity, 1996. **4**(3): p. 251-62.
42. Lee, Y., et al., *Complement component C3d-antigen complexes can either augment or inhibit B lymphocyte activation and humoral immunity in mice depending on the degree of CD21/CD19 complex engagement.* J Immunol, 2005. **175**(12): p. 8011-23.
43. Suradhat, S., et al., *Fusion of C3d molecule with bovine rotavirus VP7 or bovine herpesvirus type 1 glycoprotein D inhibits immune responses following DNA immunization.* Vet Immunol Immunopathol, 2001. **83**(1-2): p. 79-92.
44. Fries, L.F., et al., *C3b covalently bound to IgG demonstrates a reduced rate of inactivation by factors H and I.* Journal of Experimental Medicine, 1984. **160**(6): p. 1640-1655.
45. Lutz, H.U. and E. Jelezarova, *Complement amplification revisited.* Molecular

Immunology, 2006. **43**(1-2): p. 2-12.

46. Jozsi, M., *Factor H Family Proteins in Complement Evasion of Microorganisms.* Front Immunol, 2017. **8**: p. 571.
47. Aslam, M. and S.J. Perkins, *Folded-back solution structure of monomeric factor H of human complement by synchrotron X-ray and neutron scattering, analytical ultracentrifugation and constrained molecular modelling.* J Mol Biol, 2001. **309**(5): p. 1117-38.
48. Oppermann, M., et al., *The C-terminus of complement regulator Factor H mediates target recognition: evidence for a compact conformation of the native protein.* Clin Exp Immunol, 2006. **144**(2): p. 342-52.
49. Okemefuna, A.I., et al., *The regulatory SCR-1/5 and cell surface-binding SCR-16/20 fragments of factor H reveal partially folded-back solution structures and different self-associative properties.* J Mol Biol, 2008. **375**(1): p. 80-101.
50. Makou, E., A.P. Herbert, and P.N. Barlow, *Functional anatomy of complement factor H.* Biochemistry, 2013. **52**(23): p. 3949-62.
51. Upadhyay, A., et al., *Structure-Function Analysis of the C3 Binding Region of Staphylococcus aureus Immune Subversion Protein Sbi.* Journal of Biological Chemistry 2008. **283**(32): p. 22113-22120.
52. Belisle, J.T., et al., *Role of the major antigen of Mycobacterium tuberculosis in cell wall biogenesis.* Science, 1997. **276**(5317): p. 1420-2.
53. Palma, C., et al., *The Ag85B protein of Mycobacterium tuberculosis may turn a protective immune response induced by Ag85B-DNA vaccine into a potent but non-protective Th1 immune response in mice.* Cell Microbiol, 2007. **9**(6): p. 1455-65.
54. Weinrich Olsen, A., et al., *Protection of mice with a tuberculosis subunit vaccine based on a fusion protein of antigen 85b and esat-6.* Infect Immun, 2001. **69**(5): p. 2773-8.
55. Olsen, A.W., et al., *Protective effect of a tuberculosis subunit vaccine based on a fusion of antigen 85B and ESAT-6 in the aerosol guinea pig model.* Infect Immun, 2004. **72**(10): p. 6148-50.
56. Horwitz, M.A., et al., *Protective immunity against tuberculosis induced by vaccination with major extracellular proteins of Mycobacterium tuberculosis.* Proc Natl Acad Sci U S A, 1995. **92**(5): p. 1530-4.
57. Toapanta, F.R. and T.M. Ross, *Complement-mediated activation of the adaptive immune responses: role of C3d in linking the innate and adaptive immunity.* Immunol Res, 2006. **36**(1-3): p. 197-210.
58. Montoya, J., et al., *A randomized, controlled dose-finding Phase II study of the M72/AS01 candidate tuberculosis vaccine in healthy PPD-positive adults.* J Clin Immunol, 2013. **33**(8): p. 1360-75.
59. Seo, Y.B., et al., *Comparison of the immunogenicity and safety of the conventional subunit, MF59-adjuvanted, and intradermal influenza vaccines in the elderly.* Clin Vaccine Immunol, 2014. **21**(7): p. 989-96.
60. Kirkling, M.E., et al., *Notch Signaling Facilitates InVitro Generation of*

Cross-Presenting Classical Dendritic Cells. Cell reports, 2018. **23**(12): p. 3658-3672.e6.

61. Cytlak, U., et al., *Ikaros family zinc finger 1 regulates dendritic cell development and function in humans.* Nature communications, 2018. **9**(1): p. 1239.
62. Nichols, E.M., et al., *An extended mini-complement factor H molecule ameliorates experimental C3 glomerulopathy.* Kidney International, 2015. **88**(6): p. 1314-1322.
63. Alsenz, J., et al., *Phylogeny of the third component of complement, C3: analysis of the conservation of human CR1, CR2, H, and B binding sites, concanavalin A binding sites, and thiolester bond in the C3 from different species.* Developmental and Comparative Immunology, 1992. **16**(1): p. 63-76.
64. Nagar, B., et al., *X-ray crystal structure of C3d: a C3 fragment and ligand for complement receptor 2.* Science, 1998. **280**(5367): p. 1277-1281.
65. Kerr, H., et al., *Disease-linked mutations in factor H reveal pivotal role of cofactor activity in self-surface-selective regulation of complement activation.* The Journal of biological chemistry, 2017. **292**(32): p. 13345-13360.
66. Langer, A., et al., *Protein analysis by time-resolved measurements with an electro-switchable DNA chip.* Nature Communications, 2013. **4**: p. 1-8.
67. Knezevic, J., et al., *Quantitation of Affinity, Avidity, and Binding Kinetics of Protein Analytes with a Dynamically Switchable Biosurface.* Journal of the American Chemical Society, 2012. **134**(37): p. 15225-15228.
68. Franke, D., A.G. Kikhney, and D.I. Svergun, *Automated acquisition and analysis of small angle X-ray scattering data.* Nuclear Instruments & Methods in Physics Research Section a-Accelerators Spectrometers Detectors and Associated Equipment, 2012. **689**: p. 52-59.
69. Graewert, M.A., et al., *Automated Pipeline for Purification, Biophysical and X-Ray Analysis of Biomacromolecular Solutions.* Scientific Reports, 2015. **5**.
70. Yang, Y., et al., *An Engineered Complement Factor H Construct for Treatment of C3 Glomerulopathy.* Journal of the American Society of Nephrology : JASN, 2018. **29**(6): p. 1649-1661.
71. Harris, C.L., et al., *Molecular dissection of interactions between components of the alternative pathway of complement and decay accelerating factor (CD55).* The Journal of biological chemistry, 2005. **280**(4): p. 2569-78.

Figure Legends

Figure 1. Sbi-III-IV induces C3 futile consumption via the alternative complement pathway and thereby causes C3b adduct formation and C3a anaphylatoxin production.

(a) C3 activation and C3b deposition in NHS after incubation with 10 μM Sbi-III-IV, visualized using anti-C3d western blot analysis. C3b adducts formed with serum proteins are indicated. Positions of α-120 (C3) α' 110 (C3b) and α' -68 (iC3b) are indicated. The 10 minute lag-time in C3 activation we observe in the presence of excess Sbi-III-IV (10 μM) correlates with the delay reported in the natural C3 "tick-over" process, required for supplying the critical enzymatic component for the initial fluid phase Alternative Pathway (AP) C3 convertase. (b) Sbi-C3b adduct formation, visualized with anti-Sbi western blot. These adducts migrate at higher than expected molecular weights (Sbi-α' 110: ~160 kDa and Sbi-α' 68: ~120 kDa, with expected molecular weights of 125 and 83 kDa, respectively) which is caused by the high pI of the Sbi-III-IV construct (pI = 9.3). Sbi-III-IV has a molecular weight of 14.8 kDa, but migrates to ~22 kDa in SDS-polyacrylamide gel due to the positively charged electrophoresis buffer. (c) C3a anaphylatoxin production, followed using anti-C3a western blot analysis (showing only the low molecular weight region). (d) FB cleavage, monitored by anti-FB western blot analysis. (e) Concentration dependent Sbi-III-IV induced C3 consumption, studied by a rabbit erythrocytes haemolytic

assay. Rabbit erythrocytes were exposed to normal human serum pre-incubated with Sbi-III-IV (incubated, closed circles) and normal human serum with Sbi-III-IV added at the start of the experiment (not incubated, open circles). (f) Schematic representation of the relative positions of point mutations that display the most profound functional defects, K173A and R231A. (g) C3 consumption profiles of Sbi-III-IV mutants K173A and R231A. For b-e and h, one representative blot of three independent experiments was shown. For (e), four independent measurements of two experiments were shown. The mean and SD for each measurement were calculated for all datasets. Curves were fitted using non-linear variable slope (four parameters) function in GraphPad Prism.

Figure 2 Surface plasmon resonance analyses of tripartite complexes. A triply diluted concentration series (4050 to 1.8 nM) of (a) WT or (b) K173A Sbi-III-IV were co-injected with plasma purified FH, recombinant FHR-1, FHR-2, FHR-5 or FH_{19-20}. The red response curves were indicative of binding experiment in the absence of Sbi. The co-injection experiments of a fixed analyte concentration in combination with increasing Sbi concentration were depicted by increasingly dark lines. (c) Relative changes of Sbi-III-IV mediated FH (or FHR) binding to C3b. By subtracting the co-injection sensorgram (i.e. Sbi+FH) with the corresponding Sbi binding dataset (Supplementary Figure S3), the changes in FH (or FHRs) binding was deduced (Supplementary Figure S3). Changes in FH (or

FHRs) binding were expressed as the relative change, derived from dividing the Sbi mediated binding by the FH (or FHR) only control, using the response-difference values at the equilibrated binding point (173.5 *s*). Each sensorgram is representative of two experiments. Relative change curves were fitted using non-linear variable slope (four parameters) function in GraphPad Prism.

Figure 3 Functional characterization of tripartite complexes in complement AP regulation. NHS was incubated with Sbi-III-IV, in combination with specified reagents or just buffer, the consumption of AP activity was indicated by the protection of rabbit red blood cell from lysis. (a) Pre-incubation of recombinant FHR-1 or -2 with the presence or absence of Sbi-III-IV. (b) Pre-incubation of recombinant FHR-5 with the presence or absence of Sbi-III-IV. (c) Pre-incubation of recombinant FH_{19-20} or $FHR\text{-}1_{1-2}$ with the presence or absence of Sbi-III-IV. Using an ELISA assay, the ability of FHR-1, -2, -5, FH_{19-20} or $FHR\text{-}1_{1-2}$ to modulate FH binding to a C3b coated surface was studied in the presence of WT (d), no (e) or K173A Sbi-III-IV (f). C3 convertase formation in the absence (g) or presence of Sbi-III-IV (h) was assessed by flowing factor B (500 nM) and factor D (100 nM) in the presence of FH (2000 nM) or FH +FHR-1 (2000 and 200 nM) or FH+FHR-1&-5 (2000, 200 and 20 nM) across a surface amine coupled with 500 RU C3b. To form Sbi bound C3 convertase, experiments were

conducted in addition of 2000 nM of Sbi-III-IV. Detailed experimental and data processing procedures are provided in *material and methods* and Supplementary Figure S3E. (i) Percentage of intact C3b derived from continuous recording of ANS fluorescence changes between 465-475 nm spectrum. Baseline C3b breakdown curve (-) was recorded in the presence of FH and FI, interference caused by the addition of FHR-5 (+) or FHR-5 in combination of Sbi (++) was also examined. The data for FHR-1 and FHR-2 are presented in Supplementary Figure 3F. Normalized data was depicted in solid lines, simulated breakdown curves were shown as dotted-lines. Each curve represents the mean value of three independent experiments. For (a-f), the mean and standard deviation for each measurement was calculated; For (g-h), each sensorgram is representative of two experiments. For (i), simulated breakdown curves were fitted using one phase exponential decay function in GraphPad Prism.

Figure 4. Structural analysis of the Sbi-III-IV:C3d:FHR-1 tripartite complex.

SAXS solution structure analysis and EOM modeling of the Sbi-III-IV:C3d:FHR-1 tripartite complex: (a) Left panel, fit of the selected ensemble of conformers to the experimental scattering. Radius of gyration (*Rg*, middle panel), particle maximum dimension (*Dmax*, right panel), and distribution histograms of the selected conformers versus the pool. (b) Kratky plot of the tripartite complex. c) Examples of rigid body models of the selected conformers corresponding to the histogram peaks. The volume fraction of each species is indicated. The relative

positions of C3d, Sbi-III-IV and FHR-1 in the dimeric tripartite complex are indicated, with C3d in red, Sbi-IV in dark blue, Sbi-III in turquoise and FHR-1 in orange. (d) Schematic representation of the dimeric Sbi-III-IV:C3d:FHR-1 tripartite complex.

(e) Comparison of the solutions structure of wild-type Sbi-III-IV:C3d and mutated version Sbi-III-IV(K173A):C3d of the dual complex. Radius of gyration (*Rg*), particle maximum dimension (*Dmax*), and distribution histograms of the selected conformers versus the pool are shown in Supplementary Figure S4A. (f) *Ab initio* shape reconstruction shown as gray spheres in comparison to the partial crystal structure Sbi-IV:C3d (2wy8). (g) Examples of rigid body models. Complete set of models as well as flexibility assessment is presented in supplement Figures S5. C3d in shown red, Sbi-IV in dark blue, and Sbi-III in turquoise.

Figure 5. Structural and functional analysis of the Sbi-III-IV-Ag85b fusion protein. (a) Schematic structure of the Sbi-III-IV-Ag85b fusion protein (see fo details Supplementary Figure S9). (b) SAXS analysis of the fusion protein indicates a monomeric molecule with a radius of gyration of R_g=3.7 nm and maximum particle size of D_{max} =15 nm. The various molecular mass estimation range from 44 -51 kDa and are comparable with a predicted monomer mass of 50 kDa. The 10 independent *ab initio* models obtained with DAMMIF are similar to each other, and according to the χ^2 values that estimate the goodness of the fit,

1155 the final structures fit well with the experiment. More detailed modelling with
1156 Coral and EOM show that the flexibility of the missing structural information is
1157 restricted. (c) C3 activation and C3-fragment deposition in NHS after incubation
1158 with Sbi-III-IV-Ag85b (100 μM) or Ag85b (100 μM), visualized using anti-Sbi and
1159 anti-C3d western blot analysis. Resultant higher molecular weight bands with
1160 Sbi III-IV-Ag85b were identified as Sbi-III-IV-Ag85b with two covalently attached
1161 C3b α' chains; Sbi-III-IV-Ag85b with two iC3b α'-68 chains and Sbi-III-IV-Ag85b
1162 with two C3d molecules. Ag85b alone is unable to activate C3 as indicated by the
1163 presence of an intact C3 α-chain.
1164
1165 **Figure 6. Sbi-III-IV is an effective adjuvant in mice.**
1166 (a) Freshly prepared $CD21^{-/-}$ mouse serum was mixed with Sbi-III-IV-Ag85b or
1167 just Sbi-III-IV. The reaction was stopped at various time points (0, 30, 60, 120
1168 minutes). Western blot was developed with rabbit anti-C3 at 1/1000 and goat
1169 anti-rabbit at 1/2000. C3d is shown as confirmation that C3 has been activated
1170 and broken down. (N) is *Cr2*$^{-/-}$ serum incubated for 120 minutes with saline. (b)
1171 C57Bl/6 mice (groups of 6) where immunised intraperitoneally with either
1172 2.7μg Sbi-III-IV-Ag85b protein, 2μg Ag85b, or 0.7μg Sbi-III-IV plus 2μg Ag85b in
1173 150mM NaCl solution, followed by weekly bleed and boosted (day 28) before
1174 terminal bleed at day 49. Serum IgG reactivity to Ag85b was measured over time
1175 by ELISA. Sera was diluted 1/50 and the mean absorbance ± SEM of each mouse
1176 group is shown. All data has been normalised to the day 0 average of all WT mice.

1177 (c) The previous experiment was repeated in C57Bl/6 mice deficient of C3
1178 ($C3^{-/-}$)and complement receptor type I and 2 ($Cr2^{-/-}$). Data is representative of at
1179 least 2 repeats. (d) Schematic representation of the dimeric Sbi-III-IV:C3d:FHR-1
1180 solution structure providing a nidus for AP C3 convertase generation that
1181 overwhelms local complement regulators, leading to the opsonisation of the
1182 nearby antigen surface by C3 break-down products that help facilitate the
1183 co-ligation of the B cell antigen receptor (BCR) with complement receptor 2 (CR2)
1184 thereby lowering the threshold for B cell activation.
1185
1186

1

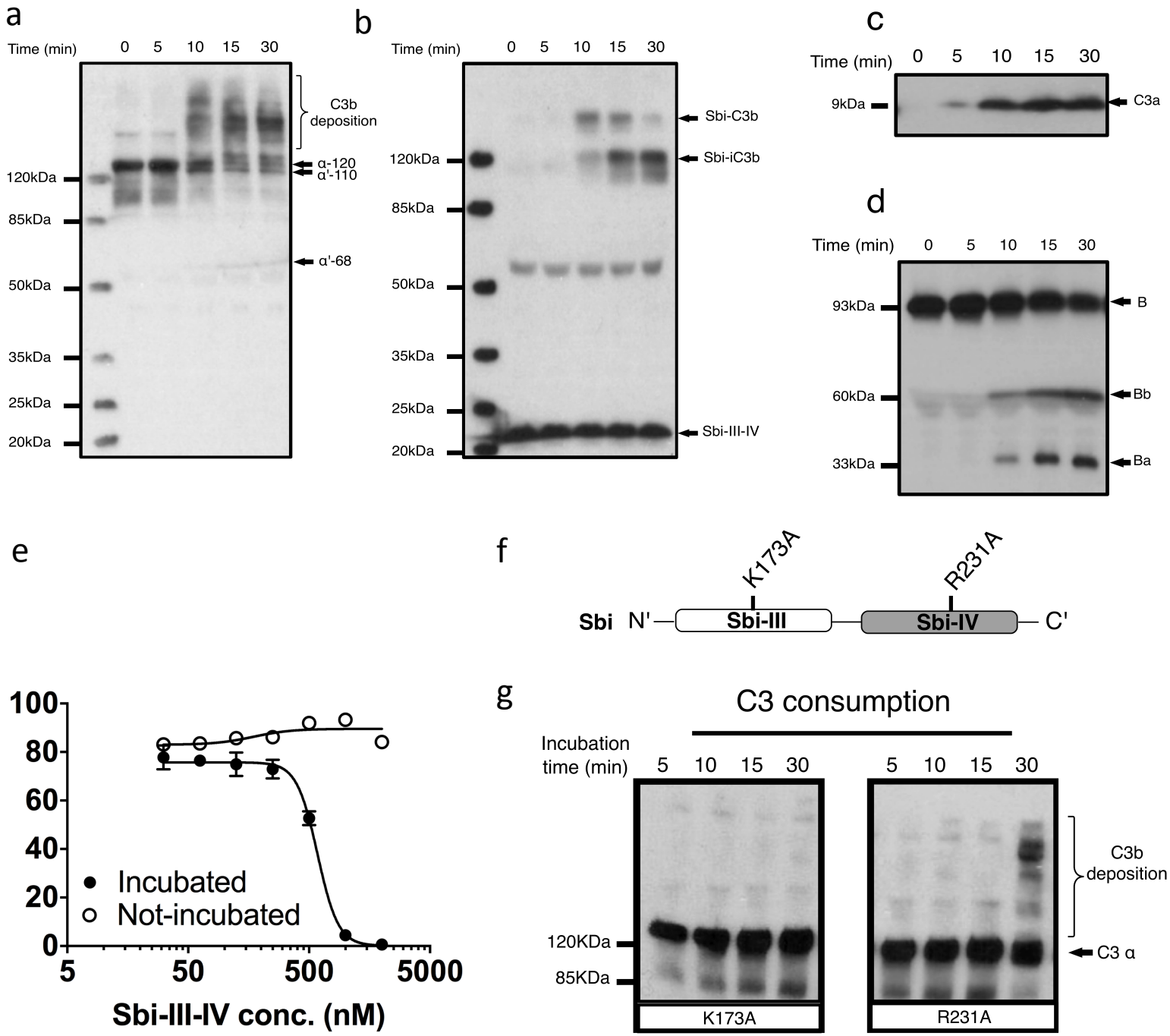
a
Time (min) 0 5 10 15 30
C3b deposition
α-120
α'-110
α'-68
120kDa
85kDa
50kDa
35kDa
25kDa
20kDa
b
Time (min) 0 5 10 15 30
Sbi-C3b
Sbi-iC3b
Sbi-III-IV
120kDa
85kDa
50kDa
35kDa
25kDa
20kDa
c
Time (min) 0 5 10 15 30
9kDa
C3a
d
Time (min) 0 5 10 15 30
93kDa
60kDa
33kDa
B
Bb
Ba
e
Lysis (%)
100
80
60
40
20
0
Incubated
Not-incubated
5
50
500
5000
Sbi-III-IV conc. (nM)
f
K173A
R231A
Sbi
N'
Sbi-III
Sbi-IV
C'
g
C3 consumption
Incubation time (min) 5 10 15 30
5 10 15 30
120KDa
85KDa
K173A
R231A
C3b deposition
C3 α

2

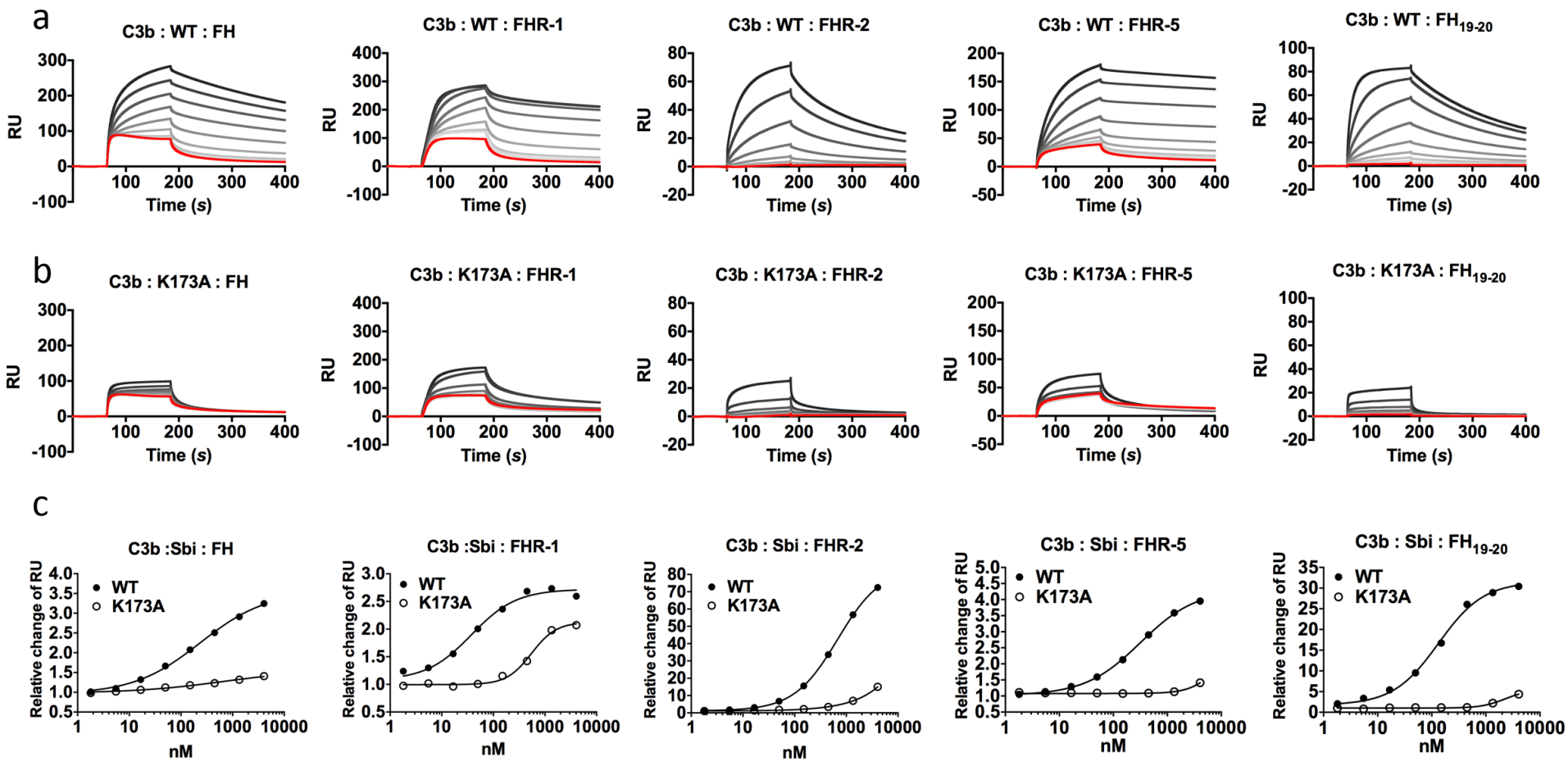
a
C3b : WT : FH
C3b : WT : FHR-1
C3b : WT : FHR-2
C3b : WT : FHR-5
C3b : WT : FH19-20
b
C3b : K173A : FH
C3b : K173A : FHR-1
C3b : K173A : FHR-2
C3b : K173A : FHR-5
C3b : K173A : FH19-20
RU
Time (s)
c
C3b :Sbi : FH
C3b :Sbi : FHR-1
C3b : Sbi : FHR-2
C3b : Sbi : FHR-5
C3b : Sbi : FH19-20
WT
K173A
Relative change of RU
nM

3

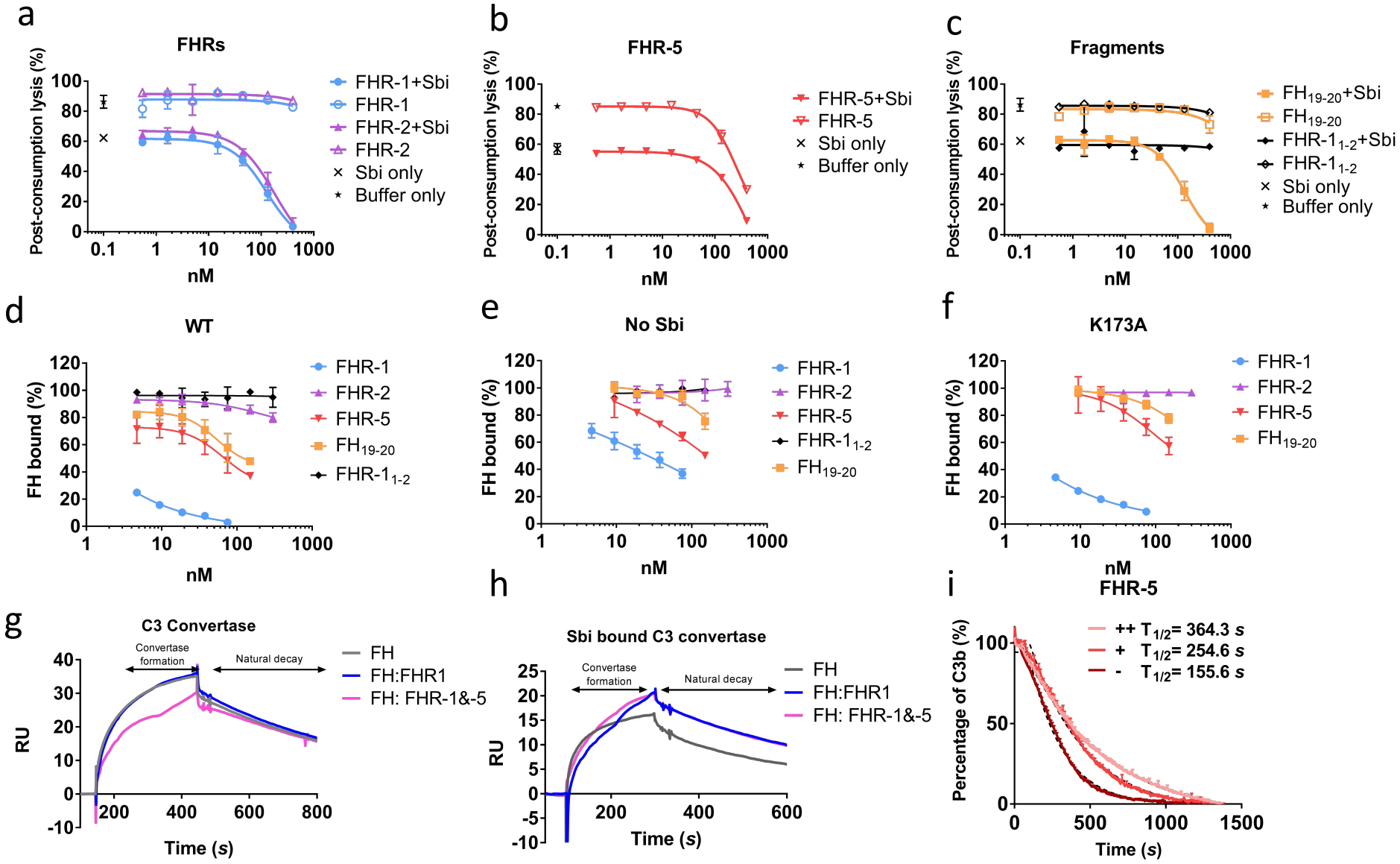
a
FHRs
Post-consumption lysis (%)
nM
FHR-1+Sbi
FHR-1
FHR-2+Sbi
FHR-2
Sbi only
Buffer only
b
FHR-5
FHR-5+Sbi
FHR-5
Sbi only
Buffer only
c
Fragments
FH19-20+Sbi
FH19-20
FHR-11-2+Sbi
FHR-11-2
Sbi only
Buffer only
d
WT
FH bound (%)
FHR-1
FHR-2
FHR-5
FH19-20
FHR-11-2
e
No Sbi
f
K173A
g
C3 Convertase
Convertase formation
Natural decay
RU
Time (s)
FH
FH:FHR1
FH: FHR-1&-5
h
Sbi bound C3 convertase
i
FHR-5
Percentage of C3b (%)
++ T1/2= 364.3 s
+ T1/2= 254.6 s
- T1/2= 155.6 s

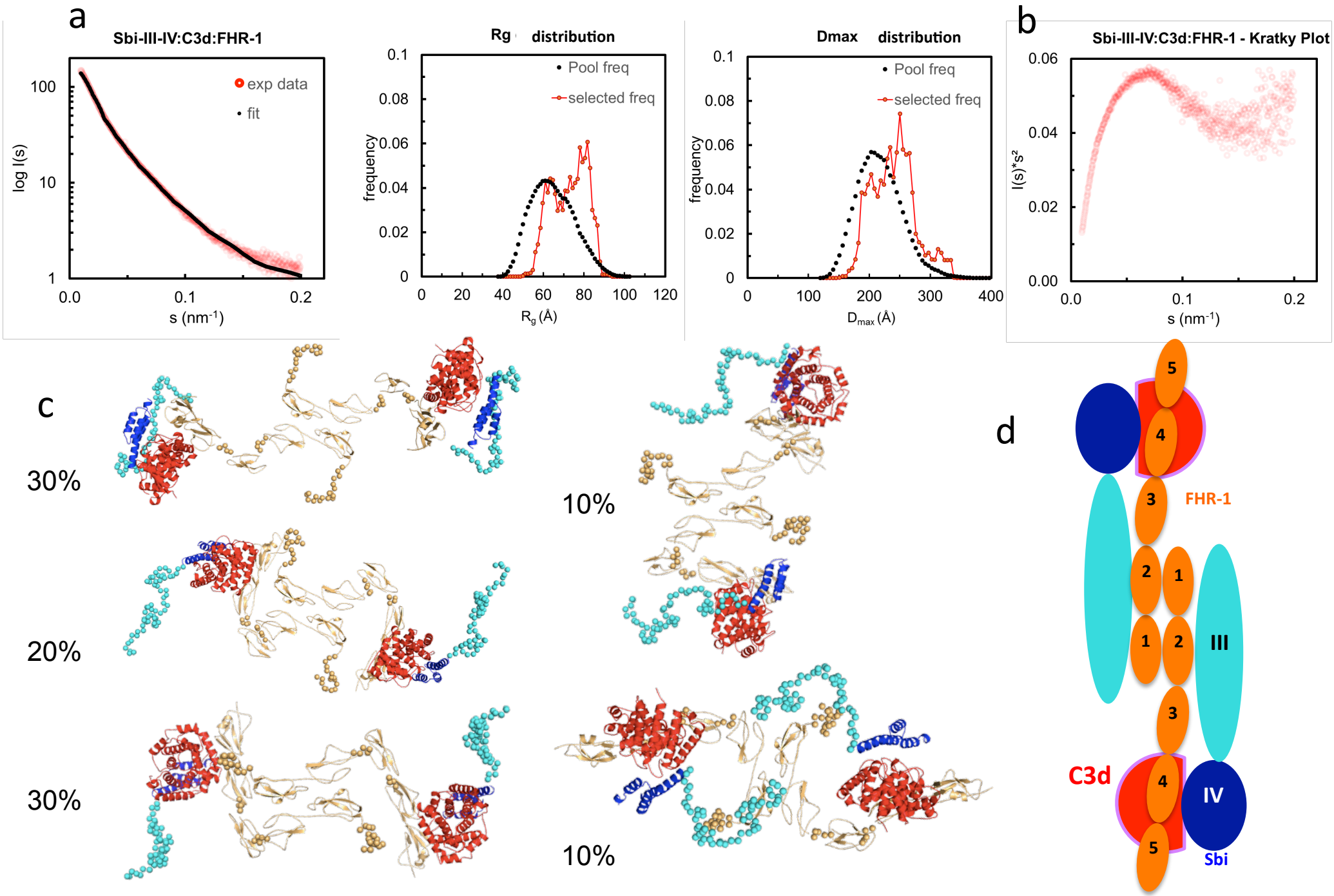
a
Sbi-III-IV:C3d:FHR-1
exp data
fit
log I(s)
s (nm-1)
Rg distribution
Pool freq
selected freq
frequency
Rg (Å)
Dmax distribution
Pool freq
selected freq
frequency
Dmax (Å)
b
Sbi-III-IV:C3d:FHR-1 - Kratky Plot
I(s)*s2
s (nm-1)
c
30%
20%
30%
10%
10%
d
5
4
3
FHR-1
2
1
1
2
III
3
C3d
4
IV
5
Sbi

4

e

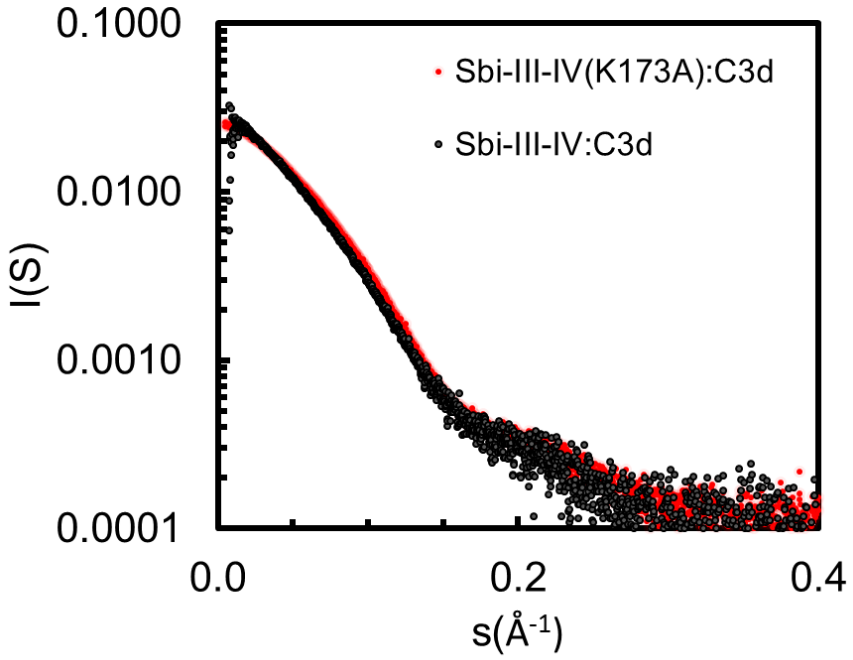
0.1000
0.0100
0.0010
0.0001
I(S)
0.0
0.2
0.4
s(Å-1)
Sbi-III-IV(K173A):C3d
Sbi-III-IV:C3d

f

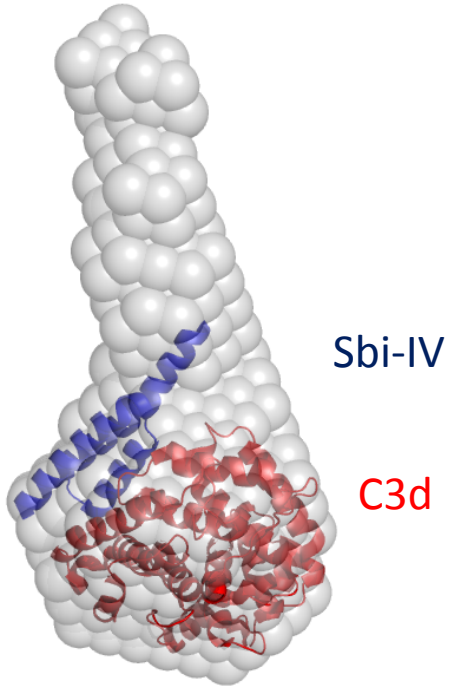
Sbi-IV
C3d

g

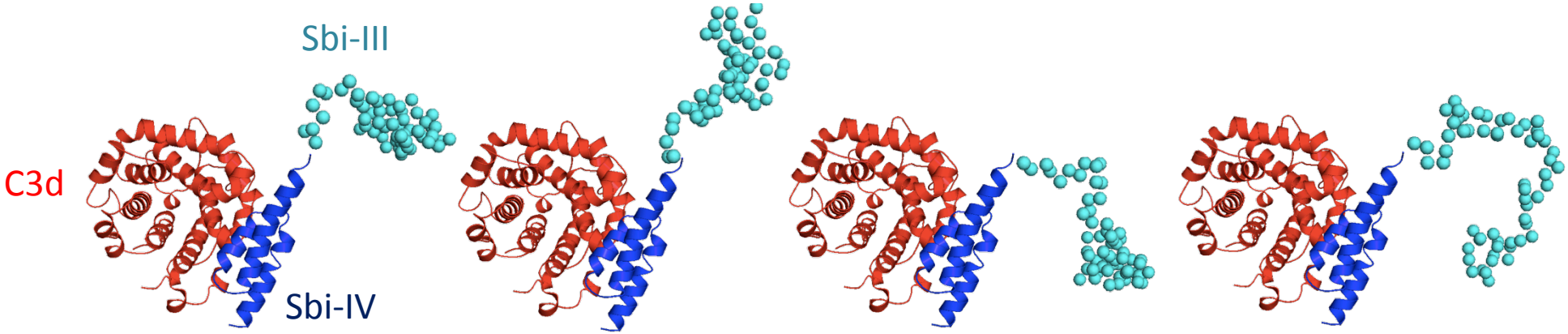
Sbi-III
C3d
Sbi-IV

5

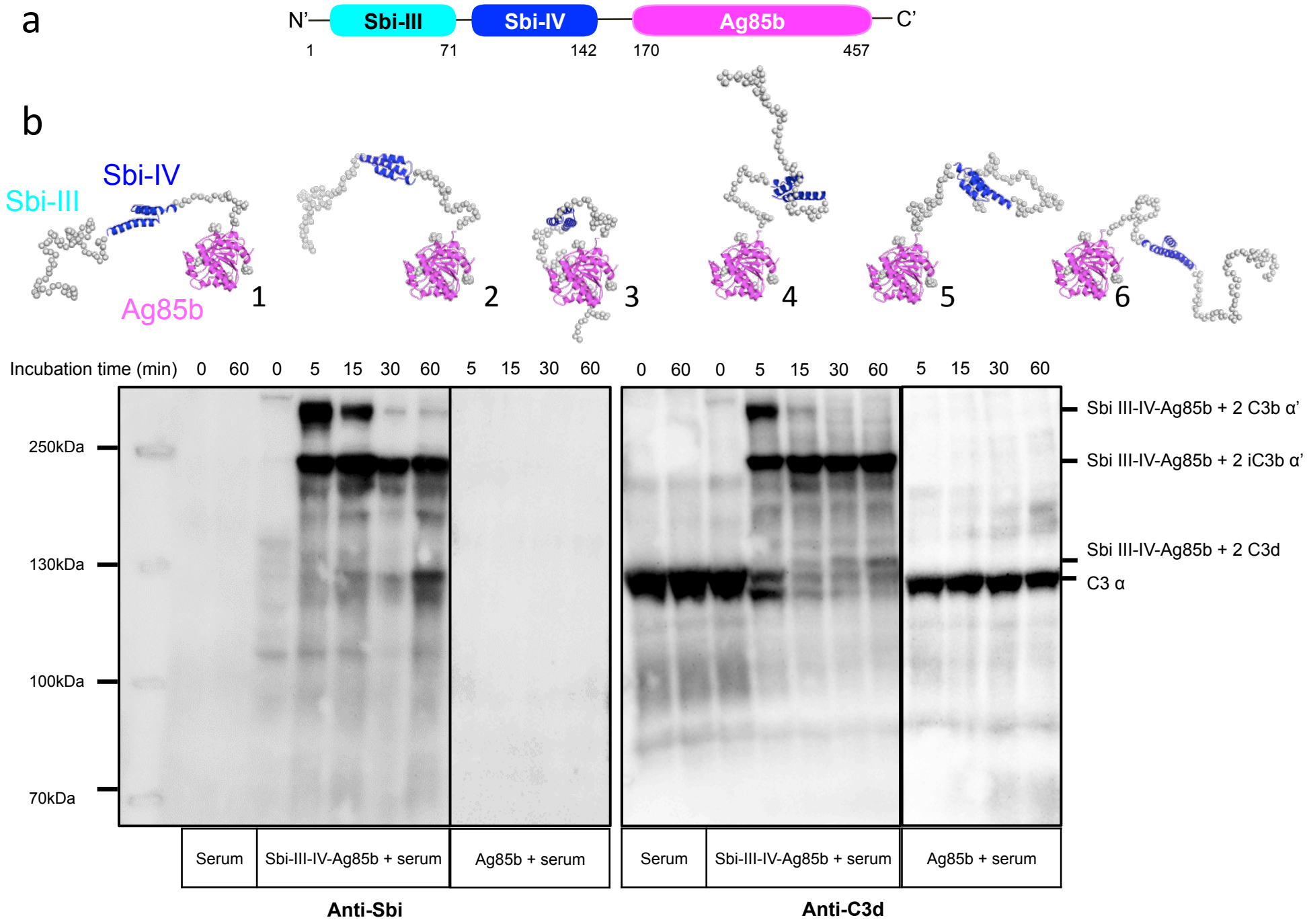
a
N'
Sbi-III
Sbi-IV
Ag85b
C'
1
71
142
170
457
b
Sbi-IV
Sbi-III
Ag85b
1
2
3
4
5
6
c
Incubation time (min) 0 60 0 5 15 30 60 5 15 30 60 0 60 0 5 15 30 60 5 15 30 60
250kDa
130kDa
100kDa
70kDa
Sbi III-IV-Ag85b + 2 C3b α'
Sbi III-IV-Ag85b + 2 iC3b α'
Sbi III-IV-Ag85b + 2 C3d
C3 α
Serum
Sbi-III-IV-Ag85b + serum
Ag85b + serum
Serum
Sbi-III-IV-Ag85b + serum
Ag85b + serum
Anti-Sbi
Anti-C3d

6

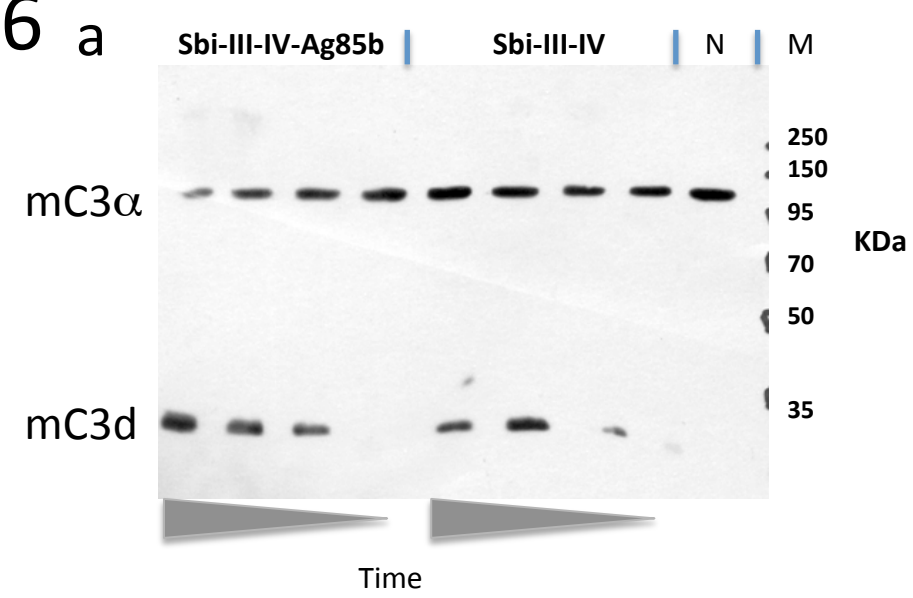
a
Sbi-III-IV-Ag85b
Sbi-III-IV
N
M
mC3α
mC3d
250
150
95
70
50
35
KDa
Time

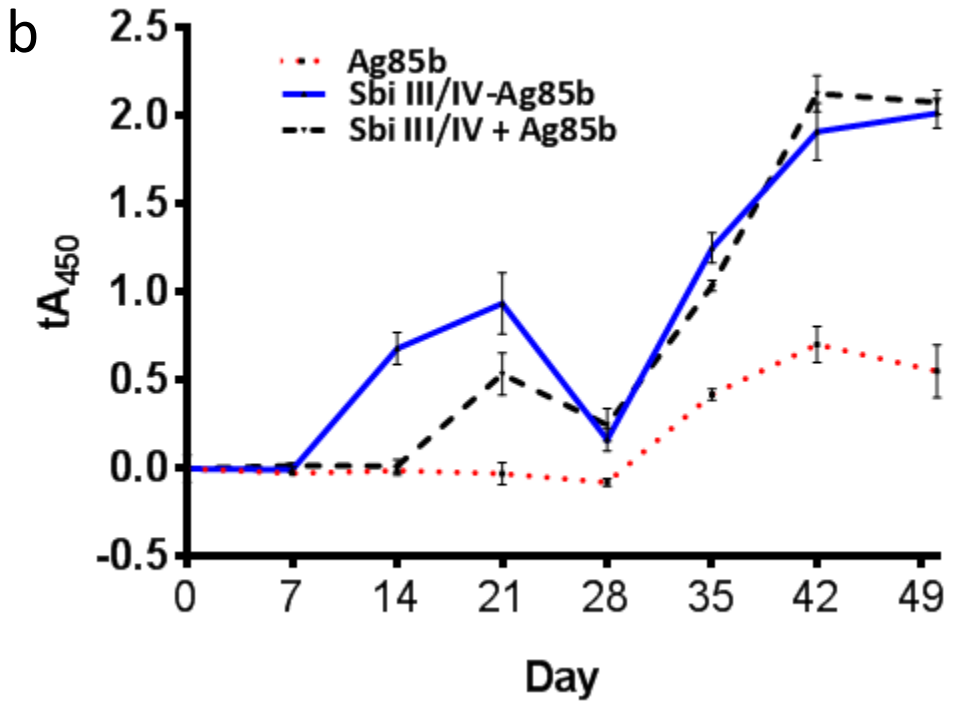
b
Ag85b
Sbi III/IV-Ag85b
Sbi III/IV + Ag85b
tA450
2.5
2.0
1.5
1.0
0.5
0.0
-0.5
0
7
14
21
28
35
42
49
Day

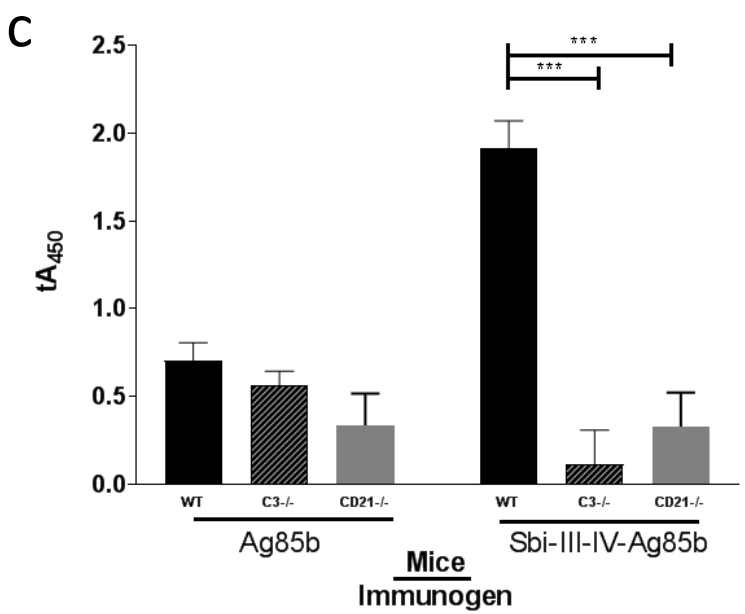
c
tA450
2.5
2.0
1.5
1.0
0.5
0.0
***
***
WT
C3-/-
CD21-/-
WT
C3-/-
CD21-/-
Ag85b
Sbi-III-IV-Ag85b
Mice
Immunogen

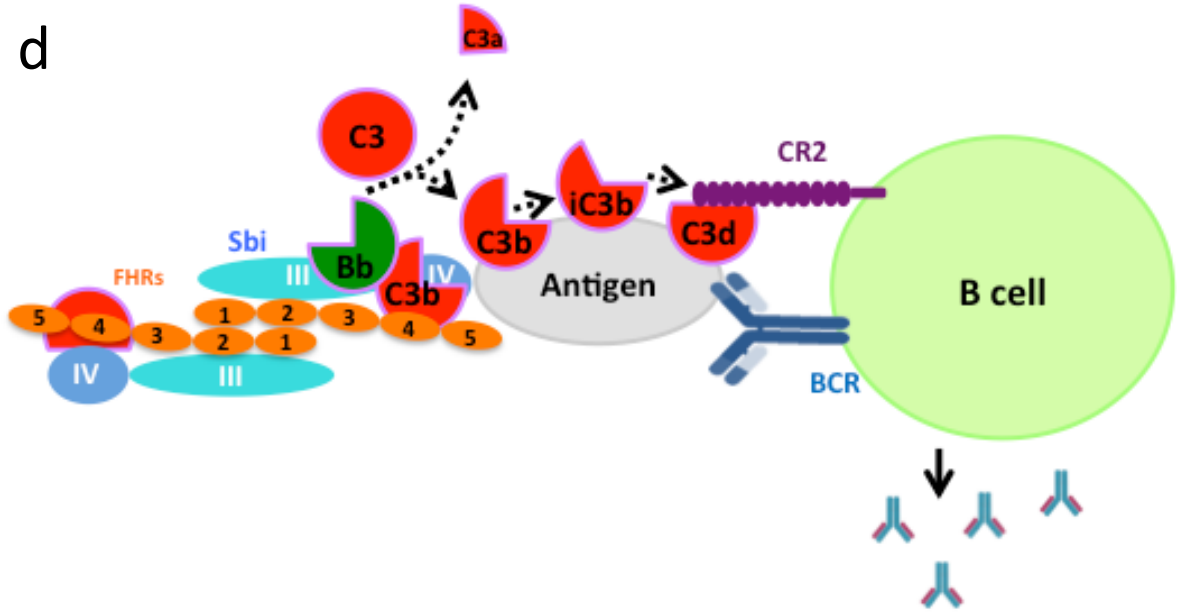
d
C3a
C3
C3b
iC3b
C3d
CR2
Sbi
FHRs
Bb
C3b
Antigen
B cell
BCR
III
IV
1
2
3
4
5

Table 1. Sbi-III-IV:C3d interaction affinity determined by *Switch*SENSE

	K_d (nM)	**k_{ON} ($M^{-1}S^{-1}$)**	**k_{OFF} (S^{-1})**
WT:C3d	5.0±0.8	$5.9±1.0×10^5$	$3.0±0.1×10^{-3}$
K173A:C3d	5.8±1.2	$5.3±0.9×10^5$	$3.0±0.4×10^{-3}$
R231:C3d	No binding		

Table 2. Sbi-III-IV:C3d complex hydrodynamic diameter determined by *Switch*SENSE

	D_H (nm) of Sbi-III-IV	**D_H (nm) of Sbi:C3d complex**
WT	4.3±0.1	6.6±0.2
K173A	3.8±0.3	5.0±0.3
R231A	4.7±0.3	No binding